JACS
JOURNAL OF THE AMERICAN CHEMICAL SOCIETY
pubs.acs.org/JACS
Article

Sterically Stabilized End-On Superoxocopper(II) Complexes and Mechanistic Insights into Their Reactivity with O−H, N−H, and C−H Substrates

Sebastian Y. Quek,[#] Suman Debnath,[#] Shoba Laxmi,[#] Maurice van Gastel, Tobias Krämer, and Jason England*

Cite This: *J. Am. Chem. Soc.* 2021, 143, 19731−19747
Read Online
ACCESS | Metrics & More | Article Recommendations | Supporting Information

ABSTRACT: Instability of end-on superoxocopper(II) complexes, with respect to conversion to peroxo-bridged dicopper(II) complexes, has largely constrained their study to very low temperatures. This limits their kinetic capacity to oxidize substrates. In response, we have developed a series of bulky ligands, Ar_3-TMPA (Ar = tpb, dpb, dtbpb), and used them to support copper(I) complexes that react with O_2 to yield $[Cu^{II}(\eta^1\text{-}O_2^{\bullet-})(Ar_3\text{-TMPA})]^+$ species, which are stable against dimerization at all temperatures. Binding of O_2 saturates at subambient temperatures and can be reversed by warming. The onset of oxygenation for the Ar = tpb and dpb systems is observed at 25 °C, and all three $[Cu^{II}(\eta^1\text{-}O_2^{\bullet-})(Ar_3\text{-TMPA})]^+$ complexes are stable against self-decay at temperatures of ≤−20 °C. This provides a wide temperature window for study of these complexes, which was exploited by performing extensive reaction kinetics measurements for $[Cu^{II}(\eta^1\text{-}O_2^{\bullet-})(tpb_3\text{-TMPA})]^+$ using a broad range of O−H, N−H, and C−H bond substrates. This includes correlation of second order rate constants (k_2) versus oxidation potentials (E_{ox}) for a range of phenols, construction of Eyring plots, and temperature-dependent kinetic isotope effect (KIE) measurements. The data obtained indicate that reaction with all substrates proceeds via H atom transfer (HAT), reaction with the phenols proceeds with significant charge transfer, and full tunneling of both H and D atoms occurs in the case of 1,2-diphenylhydrazine and 4-methoxy-2,6-di-*tert*-butylphenol. Oxidation of C−H bonds proved to be kinetically challenging, and whereas $[Cu^{II}(\eta^1\text{-}O_2^{\bullet-})(tpb_3\text{-TMPA})]^+$ can oxidize moderately strong O−H and N−H bonds, it is only able to oxidize very weak C−H bonds.

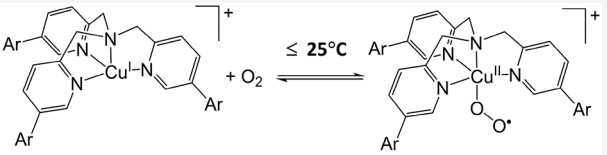

HAT reaction with a wide range of O-H, N-H and C-H substrates, including variable temperature studies

INTRODUCTION

End-on superoxocopper(II), $Cu^{II}(\eta^1\text{-}O_2^{\bullet-})$, species have been forwarded as intermediates in a wide range of O_2 activating copper-containing enzymes.[1,2] This includes the monometallic enzyme galactose oxidase (GO), wherein a $Cu^{II}(\eta^1\text{-}O_2^{\bullet-})$ species is accepted to be responsible for hydrogen atom abstraction (HAA) from a tyrosine residue to yield a catalytically crucial copper-coordinated phenoxyl radical.[3−5] There are also a number of oxygenases in which $Cu^{II}(\eta^1\text{-}O_2^{\bullet-})$ intermediates are evidenced to be responsible for initial HAA from substrate C−H bonds of moderate strength. More specifically, the noncoupled binuclear copper enzymes peptidylglycine α-hydroxylating monooxygenase (PHM), dopamine β-monooxygenase (DβM), and tyramine β-monooxygenase (TβM), which are responsible for hydroxylation of activated methylene units,[1,6,7] and the monocopper formylglycine-generating enzyme (FGE), which catalytically converts cysteine to formylglycine at an active site possessing an unusual dicysteinate-coordinated copper(I) resting state.[8,9] Of these systems, PHM and DβM are the most comprehensively studied, with some of the highlights being kinetic isotope effect (KIE) studies confirming that C−H bond oxidation occurs prior to O−O bond cleavage,[10−12] measurement of "intrinsic" substrate KIEs of 10−12,[11,13,14] evidence that hydrogen atom transfer (HAT) proceeds via quantum tunneling,[15] and an X-ray structure of PHM showing end-on coordination of O_2 to the substrate binding site Cu_M.[16] Strong support for the proposed mode of operation of the noncoupled binuclear copper enzymes, including the intermediacy of $Cu^{II}(\eta^1\text{-}O_2^{\bullet-})$ active oxidants, has been provided by DFT calculations.[17,18]

The importance of $Cu^{II}(\eta^1\text{-}O_2^{\bullet-})$ intermediates in enzymatic systems and their potential synthetic utility has spurred intensive efforts to synthesize and study the reactivity of 1:1 adducts of Cu and O_2. Although significant numbers of $Cu^{II}(\eta^1\text{-}O_2^{\bullet-})$ model complexes have now been reported (see refs 19 and 20 for comprehensive reviews of the field), exploration of their reactivity properties is not without difficulties. This is, in large part, due to their tendency to

Received: July 27, 2021
Published: November 16, 2021

https://doi.org/10.1021/jacs.1c07837
J. Am. Chem. Soc. 2021, 143, 19731−19747

collapse to thermodynamically favored species of higher nuclearity, such as peroxo-bridged dicopper(II) complexes, $Cu^{II}(\mu^2\text{-}O_2^{2-})Cu^{II}$ (Scheme 1). To retard the aforementioned

Scheme 1. Copper−O_2 Reactivity Relevant to This Study

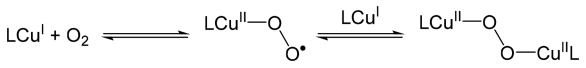

"dimerization" reaction and avoid other decay processes, such as ligand oxidation, study of $Cu^{II}(\eta^1\text{-}O_2^{\bullet-})$ complexes is overwhelmingly conducted at very low temperatures (<−80 °C). For example, in seminal work by Karlin and Zuberbühler it was shown that reaction of $[Cu^{I}(TMPA)(NCMe)]^+$ (Chart 1) with O_2 at temperatures between −75 and −90 °C rapidly

Chart 1. Selected Ligands That Have Been Used To Support $Cu^{II}(\eta^1\text{-}O_2^{\bullet-})$ Complexes

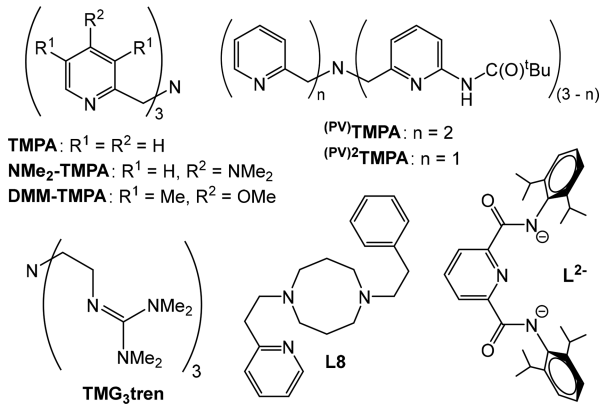

forms the corresponding $Cu^{II}(\mu^2\text{-}O_2^{2-})Cu^{II}$ complex.[21,22] The species $[Cu^{II}(\eta^1\text{-}O_2^{\bullet-})(TMPA)]^+$ was observed as a transient intermediate, using stopped-flow kinetics, but low temperatures of −135 °C were required to accumulate significant amounts of it.[23] Even then, it was obtained as a mixture with, and slowly converts to, the corresponding $Cu^{II}(\mu^2\text{-}O_2^{2-})Cu^{II}$ complex.

The simplest method of prohibiting formation of 2:1 adducts of Cu and O_2 (and higher nuclearity species) is to employ sterically encumbered ligands. This has proven particularly successful for monoanionic bidentate and tridentate ligand architectures, which tend to favor formation of side-on bound (η^2) 1:1 adducts of Cu and O_2. These $Cu(\eta^2\text{-}O_2)$ species are (in general) much more stable than their $Cu^{II}(\eta^1\text{-}O_2^{\bullet-})$ analogues, and concordantly, several $Cu^{II}(\eta^2\text{-}O_2^{\bullet-})$ or $Cu^{III}(\eta^2\text{-}O_2^{2-})$ complexes have been isolated and crystallographically characterized.[24−30] Unfortunately, this comparatively high stability equates to low intermolecular reactivity. Indeed, the only exception, Beltey's dipyrrin-supported $Cu^{II}(\eta^2\text{-}O_2^{\bullet-})$ complex, is believed to react with substrates via a thermally driven isomerization to the corresponding $Cu^{II}(\eta^1\text{-}O_2^{\bullet-})$ species.[27]

Sterically encumbered ligands are also effective at stabilizing $Cu^{II}(\eta^1\text{-}O_2^{\bullet-})$ moieties, with the most graphic demonstration being Schindler and co-workers' synthesis of $[Cu^{II}(\eta^1\text{-}O_2^{\bullet-})(TMG_3\text{-tren})]^+$ (Chart 1).[31] Not only was this complex fully stable against formation of higher nuclearity species, but it was generated via a fully reversible oxygenation reaction, and the superoxocopper(II) complex was sufficiently stable for crystallographic characterization.[32,33] Unfortunately, like most other sterically stabilized systems,[34,35] it was found to display limited HAA reactivity with substrates.[36] This may not be due to steric factors alone, with the high basicity of the guanidine donors likely to significantly impact reactivity. Consistent with this notion, Tolman's complex $[Cu^{II}(\eta^1\text{-}O_2^{\bullet-})(L)]^-$, supported by a dianionic 2,6-dicarboxamidopyridine ligand (Chart 1),[35] performs HAA only from weak O−H bonds. In other circumstances, it tends to favor nucleophilic reaction (primarily protonation).[37−39]

To date, the most diverse array of reactivity displayed by a single system was reported for Itoh's complex $[Cu^{II}(\eta^1\text{-}O_2^{\bullet-})(L8)]^+$ (Chart 1).[40] It oxidizes a range of electron transfer agents, which allowed estimation of its reduction potential, it performs oxo-atom transfer to phosphines, and it reacts with phenols via protonolysis and TEMPO-H to yield the corresponding hydroperoxocopper(II) complex.[41] In addition, $[Cu^{II}(\eta^1\text{-}O_2^{\bullet-})(L8)]^+$ undergoes self-decay via intramolecular hydroxylation of the benzylic position of its pendant ethylbenzene substitutent, for which a KIE and Eyring parameters were measured.[42,43] The unique reactivity of this system has been attributed to the close resemblance of its pseudo-tetrahedral coordination geometry to that of the O_2 activating Cu_M site of noncoupled binuclear copper monooxygenases.[40]

However, the most extensive substrate reactivity studies reported for $Cu^{II}(\eta^1\text{-}O_2^{\bullet-})$ model complexes are those of Karlin and co-workers, which revolve around derivatives of the TMPA ligand system (Chart 1). They demonstrated that introduction of electron donating[44−46] and hydrogen bond donor[23,47] functionality onto this ligand framework can "stabilize" the $Cu^{II}(\eta^1\text{-}O_2^{\bullet-})$ moiety by slowing or eliminating conversion to $Cu^{II}(\mu^2\text{-}O_2^{2-})Cu^{II}$ complexes. This provided a means to study reaction of the corresponding $Cu^{II}(\eta^1\text{-}O_2^{\bullet-})$ complexes with a wide array of substrates. For instance, extensive mechanistic studies for reaction of $[Cu^{II}(\eta^1\text{-}O_2^{\bullet-})(DMM\text{-}TMPA)]^+$ with phenolic substrates were conducted.[46] This included measurement of rate constants over a 15 °C temperature range, from −85 to −100 °C, which allowed construction of an Eyring plot. More recently, introduction of H-bond donor substituents at the 6-position of the pyridine donors was shown to significantly enhance reactivity. A single pivaloyl functional group, giving $^{(PV)}$TMPA (Chart 1), allows HAA from the weak C−H bonds of 1-benzyl-1,4-dihydronicotinamide (BNAH) and 1,3-dimethyl-2,3-dihydrobenzimidazole (BzImH) and the comparatively strong O−H bond of 4-methoxyphenol.[23,47] Furthermore, the inclusion of two pivaloyl groups, giving $^{(PV)2}$TMPA (Chart 1), allows reaction with the stronger C−H bonds of dihydroanthracene and fluorene at −135 °C.[48]

With the aforementioned factors in mind, we sought to stabilize a TMPA-supported $Cu^{II}(\eta^1\text{-}O_2^{\bullet-})$ complex via introduction of bulky substituents, but in such a way that steric inhibition of reaction with substrates is minimized. To this end, we installed a series of bulky aryl substituents onto the 5-position of the pyridine rings to give the Ar_3-TMPA ligands (Figure 1). The formation and stability of the resulting $[Cu^{II}(\eta^1\text{-}O_2^{\bullet-})(Ar_3\text{-}TMPA)]^+$ complexes, where Ar = 2,4,6-triphenylbenzene (tpb), 2,6-diphenylbenzene (dpb), and 2,6-di(4-*tert*-butylphenyl)benzene (dtbpb), plus their reactivity with a broad range of O−H, N−H, and C−H bond substrates are detailed herein.

https://doi.org/10.1021/jacs.1c07837
J. Am. Chem. Soc. 2021, 143, 19731−19747

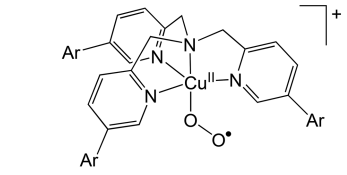

$[Cu^{II}(\eta^1\text{-}O_2^{\bullet-})(Ar_3\text{-TMPA})]^+$

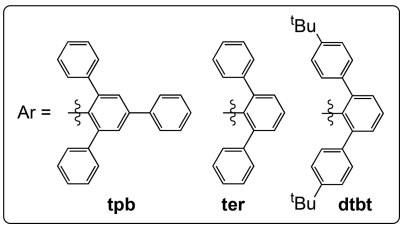

Figure 1. $Cu^{II}(\eta^1\text{-}O_2^{\bullet-})$ complexes studied herein.

RESULTS AND DISCUSSION

The Ar_3-TMPA (Ar = tpb, dpb, dtbpb) ligands described in this study were synthesized by Suzuki cross-coupling of Br_3-TMPA with the pertinent aryl boronic acids (Scheme S1). Copper(I) complexes of Ar_3-TMPA, employed in the oxygenation studies described below, were prepared by combination with the salt $[Cu^I(NCMe)_4][B(C_6F_5)_4]$ in tetrahydrofuran solution. Upon the basis of ^{1}H NMR spectra recorded in THF-d_8 solution, wherein the pyridyl donors are equivalent and there are no MeCN co-ligands , they are formulated as four-coordinate $[Cu^I(Ar_3\text{-TMPA})][B(C_6F_5)_4]$ (Ar = tpb, dpb, and dtbpb). The copper(II) complexes $[Cu^{II}(Ar_3\text{-TMPA})(NCMe)](Y)_2$ ($Y^- = ClO_4^-$ or TfO^-) were prepared in a similar fashion, by reaction of ligand with either $Cu^{II}(ClO_4)_2\cdot 6H_2O$ or $Cu^{II}(OTf)_2$ in acetonitrile solution. Attempts to grow crystals suitable for X-ray crystallography were only successful for the copper(II) complexes. As expected, the dicationic components of $[Cu^{II}(tpb_3\text{-TMPA})(NCMe)](ClO_4)_2$, $[Cu^{II}(dpb_3\text{-TMPA})(NCMe)](ClO_4)_2$, and $[Cu^{II}(dtbpb_3\text{-TMPA})(NCMe)](OTf)_2$ all display trigonal bipyramidal geometries (τ_5[49] = 0.97, 0.80, and 1.00, respectively), with the TMPA ligands coordinating in a tripodal tetradentate fashion and the remaining axial coordination site filled by an acetonitrile ligand (Figures 2 and S16–S18). Crystallographic data and selected structural parameters are listed in the Supporting Information in Tables S1–S4.

It is clear from the X-ray crystal structures that the bulky Ar substituents primarily point away from the metal center, and only in the case of $dtbpb_3$-TMPA do they crowd the MeCN-occupied axial coordination site to a readily appreciable extent. Instead of projecting vertically, parallel to the Cu–NCMe axis, the steric bulk is predominantly oriented laterally, perpendicular to the Cu–NCMe axis. It was anticipated that this would provide interdonor repulsion while minimizing the decrease in donor strength that usually accompanies introduction of steric bulk.

Although the respective average $Cu–N_{pyridine}$ bond lengths in $[Cu^{II}(tpb_3\text{-TMPA})(NCMe)]^{2+}$, $[Cu^{II}(dpb_3\text{-TMPA})(NCMe)]^{2+}$ and $[Cu^{II}(dtbpb_3\text{-TMPA})(NCMe)]^{2+}$ of 2.067(3), 2.071(5), and 2.060(4) Å may be marginally longer than the corresponding distance of 2.042(4) Å in the parent compound $[Cu^{II}(TMPA)(NCMe)]^{2+}$,[50] the values are sufficiently similar to argue that the impact of the aryl substituents is minimal. In contrast, introduction of phenyl rings onto the 6-position of the pyridine donors in the parent TMPA ligand causes elongation of the average $Cu–N_{pyridine}$ distance in the corresponding copper(II) complex, $[Cu^{II}(6\text{-}Ph_3\text{-TMPA})(NCMe)]^{2+}$, to 2.108(7) Å.[51] This represents an obvious weakening of pyridine-to-Cu donation.

Cyclic voltammetry measurements (Figure S19, Table 1) are consistent with the assertion that the aryl substituents in the $[Cu^{II}(Ar_3\text{-TMPA})(NCMe)]^{2+}$ complexes do not significantly weaken with the donor ability of the pyridine rings. More specifically, the half-wave potentials ($E_{1/2}$) of the Cu^{II}/Cu^I redox couples of the Ar = tpb and dpb complexes (−0.39 and −0.41 V vs Fc^+/Fc^0, respectively) are essentially identical to

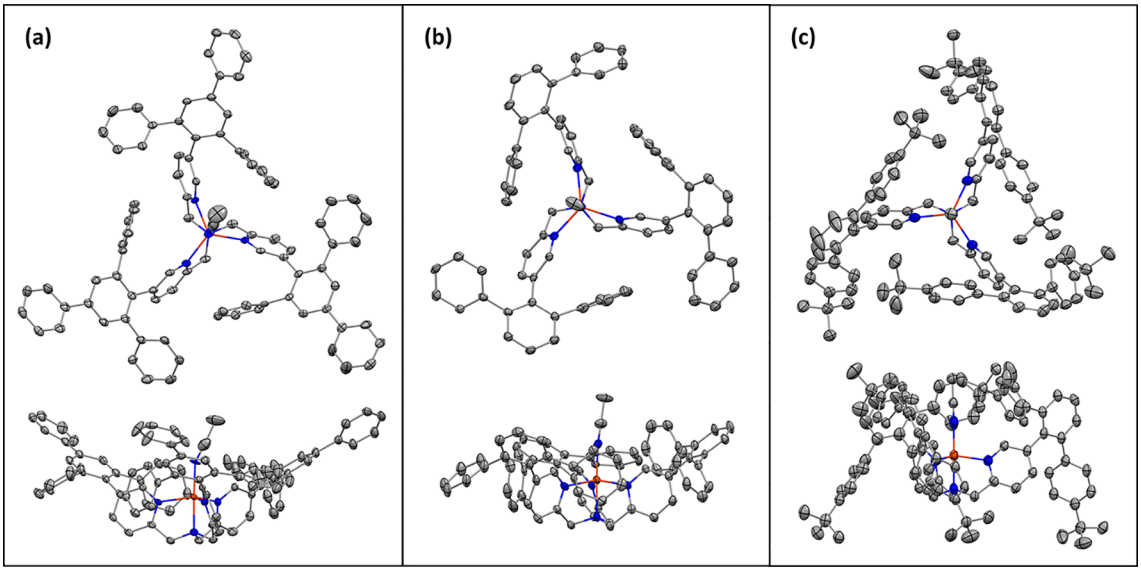

Figure 2. Top and side views (above and below, respectively) of the X-ray crystal structures of (a) $[Cu^{II}(tpb_3\text{-TMPA})(NCMe)](ClO_4)_2$, (b) $[Cu^{II}(dpb_3\text{-TMPA})(NCMe)](ClO_4)_2$, and (c) $[Cu^{II}(dtbpb_3\text{-TMPA})(NCMe)](OTf)_2$, depicted using 50% thermal ellipsoids. Hydrogen atoms, counteranions, and solvent molecules have been omitted for clarity. Gray, blue, and orange spheroids correspond to carbon, nitrogen, and copper atoms, respectively.

https://doi.org/10.1021/jacs.1c07837
J. Am. Chem. Soc. 2021, 143, 19731–19747

Table 1. Half-Wave Potentials ($E_{1/2}$) of the Cu^{II}/Cu^{I} Redox Couples of $[Cu^{II}(Ar_3\text{-TMPA})(NCMe)]^{2+}$ (Ar = tpb, dpb, and dtbpb) and Selected Complexes[a]

$[Cu^{II}(L)(NCMe)]^{2+}$, L =	$E_{1/2}$ vs Fc^{+}/Fc^{0} (V)	ref
tpb_3-TMPA	−0.39	this work
dpb_3-TMPA	−0.41	this work
$dtbpb_3$-TMPA	−0.32	this work
TMPA	−0.40	44, 51
6-Ph_3-TMPA	−0.10	51

[a]All data was recorded at 298 K, in MeCN solution using 0.1 M NBu_4PF_6 as an electrolyte, and is quoted versus the Fc^{+}/Fc^{0} redox couple. $E_{1/2} = (E_{pc} + E_{pa})/2$.

the value of −0.40 V reported for $[Cu^{II}(TMPA)(NCMe)]^{2+}$.[44,51] The $E_{1/2}$ of −0.32 V measured for the Ar = dtbpb is more positive than the aforementioned values and indicates destabilization of the Cu^{II} oxidation state, but this cathodic shift is small compared to systems possessing substituents on the 6-position of the pyridine donors. For example, the corresponding $E_{1/2}$ value for $[Cu^{II}(6\text{-}Ph_3\text{-}TMPA)(NCMe)]^{2+}$ is −0.10 V.[51]

Superoxocopper(II) Complex Formation. It was found that pale yellow solutions of all three $[Cu^{I}(Ar_3\text{-TMPA})][B(C_6F_5)_4]$ copper(I) complexes react rapidly with O_2 at −80 °C in a broad range of organic solvents, including THF, MeTHF, acetone, toluene, and diethyl ether, to yield green species. Saturation of O_2 binding took less than 10 s in THF. The UV−vis spectra of the three green species closely resemble one another, with three prominent bands centered (λ_{max}) at approximately 430, 580, and 760 nm (Figure 3a and Table 2). These features are highly diagnostic of end-on

Table 2. Summary of the UV−Visible and Resonance Raman Spectral Features of $[Cu^{II}(\eta^1\text{-}O_2^{\bullet-})(Ar_3\text{-TMPA})]^{+}$ (Ar = tpb, dpb, and dtbpb), and Second Order Rate Constants (k_2, M^{-1} s^{-1}) for Reaction of These Complexes with 4-Methoxy-2,6-di-*tert*-butylphenol (MeO-ArOH) at −70 °C

Ar	λ_{max}, nm (ε_{max}, M^{-1} cm^{-1})[a]	ν(O−O)[b] (cm^{-1})	ν(Cu−O)[b] (cm^{-1})	k_2 (M^{-1} s^{-1})
tpb	429 (3740)	1127 {−58}	482 {−23}	0.90(5)
	583 (1200)			
	760 (1700)			
dpb	430(3950)	1126 {−63}	467 {−18}	0.93(5)
	584 (1150)			
	760 (1690)			
dtbpb	434 (3660)	1119 {−60}	?	0.042(2)
	573 (1260)			
	768 (2080)			

[a]Recorded in THF solution, at −80 °C. [b]Values in braces are the shifts in peak position observed upon ^{18}O-labeling.

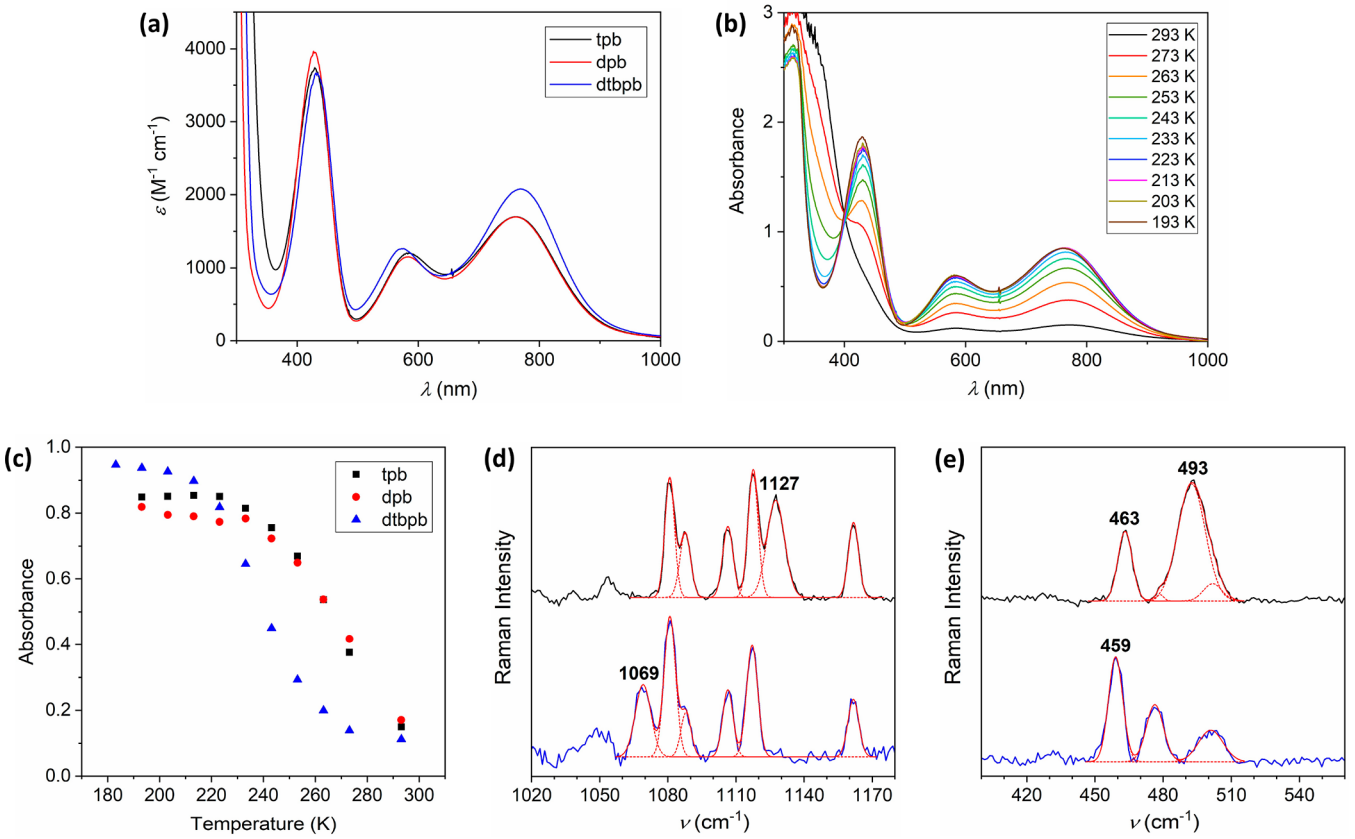

Figure 3. (a) UV−vis spectra of $[Cu^{II}(\eta^1\text{-}O_2^{\bullet-})(Ar_3\text{-TMPA})]^{+}$ (Ar = tpb, dpb, and dtbpb), recorded in THF solution at −80 °C. (b) UV−vis spectra of O_2 saturated THF solutions of $[Cu^{I}(tpb_3\text{-TMPA})]^{+}$ (~0.5 mM) and (c) absorbances at the 760−771 nm λ_{max} of all three $[Cu^{II}(\eta^1\text{-}O_2^{\bullet-})(Ar_3\text{-TMPA})]^{+}$ (Ar = tpb, dpb, and dtbpb) complexes, measured at 20 °C and regular intervals over the temperature range of 0 to −90 °C. Expansions of the (d) ν(O−O) and (e) ν(Cu−O) containing regions of resonance Raman spectra (λ_{ex} = 405 nm) of frozen d_8-THF solutions of $[Cu^{II}(\eta^1\text{-}^{16}O_2^{\bullet-})(tpb_3\text{-TMPA})]^{+}$ (black lines) and $[Cu^{II}(\eta^1\text{-}^{18}O_2^{\bullet-})(tpb_3\text{-TMPA})]^{+}$ (blue lines). Solid and dashed red lines correspond to spectral simulations and Gaussians that comprise the simulations, respectively.

https://doi.org/10.1021/jacs.1c07837
J. Am. Chem. Soc. 2021, 143, 19731−19747

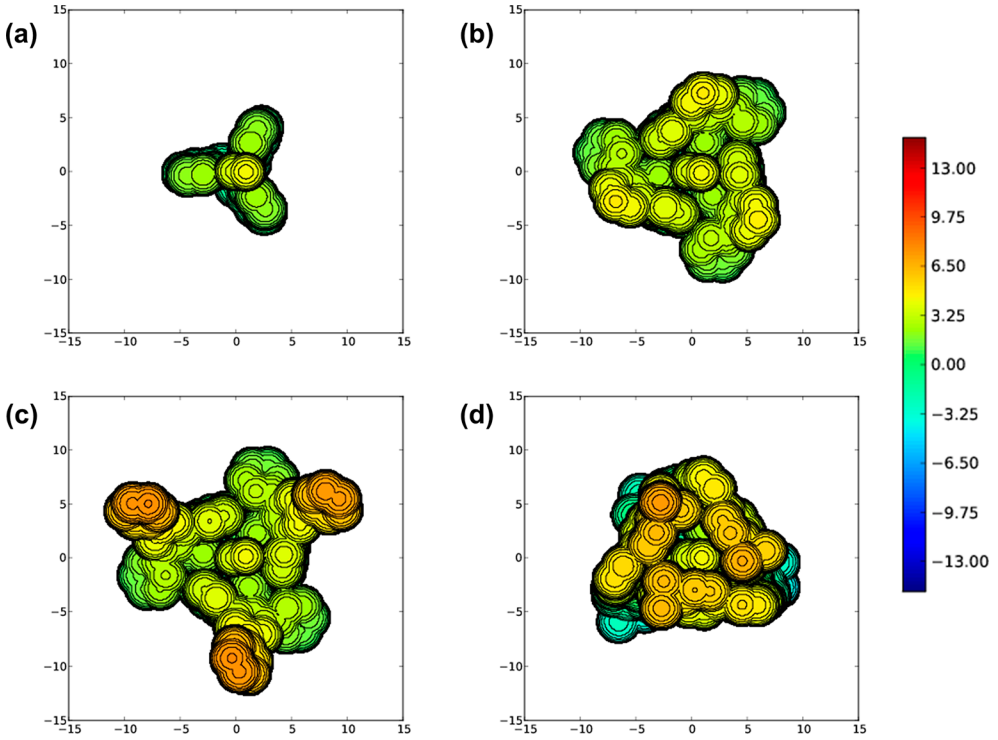

Figure 4. Topographic steric maps derived from the DFT calculated geometry optimized structures of the triplet (S = 1) ground states of (a) $[Cu^{II}(\eta^1\text{-}O_2^{\bullet-})(TMPA)]^+$, (b) $[Cu^{II}(\eta^1\text{-}O_2^{\bullet-})(dpb_3\text{-}TMPA)]^+$, (c) $[Cu^{II}(\eta^1\text{-}O_2^{\bullet-})(tpb_3\text{-}TMPA)]^+$, and (d) $[Cu^{II}(\eta^1\text{-}O_2^{\bullet-})(dtbpb_3\text{-}TMPA)]^+$. In all cases, the copper ion and $Cu\text{–}N_{amine}$ bond are defined as the origin and z-axis, respectively. The distance above and below the origin (along the z-axis) is color-coded, according to the figure key.

superoxocopper(II) complex formation and are very similar to those of the parent complex $[Cu^{II}(\eta^1\text{-}O_2^{\bullet-})(TMPA)]^+$ (λ_{max} = 410 and 747 nm, with respective ε_{max} = 4000 and 1000 M^{-1} cm^{-1}).[21]

Confirmation of assignment of these green species as $[Cu^{II}(\eta^1\text{-}O_2^{\bullet-})(Ar_3\text{-}TMPA)]^+$ complexes was provided by resonance Raman spectroscopy (Figure 3d,e and Figures S23–S28). Using laser excitation at a wavelength (λ_{ex}) of 405 nm, vibrational bands were observed at 1127–1119 cm^{-1} and found to shift to 1069–1059 cm^{-1} upon labeling with $^{18}O_2$ (Table 2). This is very similar to the O–O stretching frequencies, ν(O–O), reported for other $Cu^{II}(\eta^1\text{-}O_2^{\bullet-})$ complexes, and the observed isotope shifts ($\Delta\nu$ = 58–63 cm^{-1}) are consistent with assignment as such.[19,20] These ν(O–O) values are distinct from those recorded for $Cu^{II}(\eta^2\text{-}O_2^{\bullet-})$ complexes, which tend to appear at ∼1000 cm^{-1}.[19] It should be noted that whereas the $[Cu^{II}(\eta^1\text{-}O_2^{\bullet-})(Ar_3\text{-}TMPA)]^+$ complexes produced with natural abundance O_2 exhibit a single ν(O–O) band, the $^{18}O_2$-labeled isotopologues of the Ar = dpb and dtbpb variants possess two readily resolved peaks of unequal intensity. The same may be true of the Ar = tpb complex, but the ^{18}O-labeled data is not of sufficient resolution to definitively determine whether this is the case or not. Regardless, observations of this type have precedence and are attributed to Fermi resonance with a nonenhanced vibrational mode.[23,48]

The Cu–O stretching modes, ν(Cu–O), are also readily discerned in the resonance Raman spectra of the complexes. In the cases of $[Cu^{II}(\eta^1\text{-}O_2^{\bullet-})(tpb_3\text{-}TMPA)]^+$ and $[Cu^{II}(\eta^1\text{-}O_2^{\bullet-})(dpb_3\text{-}TMPA)]^+$ they present as Fermi doublets. Upon $^{18}O_2$ labeling, they shift to lower energy and appear as single bands. The situation is more complex for $[Cu^{II}(\eta^1\text{-}O_2^{\bullet-})(dtbpb_3\text{-}TMPA)]^+$ because several bands are observed in both the natural abundance O_2 and $^{18}O_2$-labeled compounds (Figure S28). This is presumed to be, at least in part, due to Fermi resonance. However, the close-spacing of these features, combined with experimental error and limitations of the data, renders accurate assignment very difficult. Nevertheless, the ν(Cu–O) values of 482 and 467 cm^{-1} observed for the Ar = tpb and dpb complexes, respectively, fall within the expected range for $Cu^{II}(\eta^1\text{-}O_2^{\bullet-})$ species and below that of their side-on bound congeners, $Cu(\eta^2\text{-}O_2)$, which are reported have higher ν(Cu–O) of around 490–560 cm^{-1}.[19]

To probe the spin-states of the $[Cu^{II}(\eta^1\text{-}O_2^{\bullet-})(Ar_3\text{-}TMPA)]^+$ complexes in fluid solution, Evans' NMR measurements were performed in THF-d_8 at −80 °C. This yielded effective magnetic moments (μ_{eff}) of 3.28, 2.99, and 3.03 μ_B for Ar = tpb, dpb, and dtbpb, respectively, which are all very close to the spin-only expectation value (2.83 μ_B) for an S = 1 system. Thus, it can be inferred that the unpaired electrons on the Cu^{II} and $O_2^{\bullet-}$ ions ferromagnetically couple with one another. To verify this conclusion, DFT calculations were performed for the $[Cu^{II}(\eta^1\text{-}O_2^{\bullet-})(Ar_3\text{-}TMPA)]^+$ complexes. More specifically, attempts were made to assess the relative stabilities of the S = 0 and 1 states for both $Cu^{II}(\eta^1\text{-}O_2^{\bullet-})$ and $Cu^{II}(\eta^2\text{-}O_2^{\bullet-})$ structures. For all three Ar groups, the S = 1 $Cu^{II}(\eta^1\text{-}O_2^{\bullet-})$ structures were calculated to be lowest in energy, with the corresponding open-shell M_S = 0 $Cu^{II}(\eta^1\text{-}O_2^{\bullet-})$, closed-shell S = 0 $Cu^{II}(\eta^1\text{-}O_2^{\bullet-})$, and S = 0 $Cu^{II}(\eta^2\text{-}O_2^{\bullet-})$ states being ≥ 4.4, 20.8, and 19.0 $kcal^{-1}$ mol^{-1} higher in energy, respectively (Figure S29). Attempts to locate a S = 1 $Cu^{II}(\eta^2\text{-}O_2^{\bullet-})$ optimized geometry converged, in all cases, to the $Cu^{II}(\eta^1\text{-}O_2^{\bullet-})$ ground state. Thus, the DFT calculations support the experimental findings and confirm that the S = 1

https://doi.org/10.1021/jacs.1c07837
J. Am. Chem. Soc. 2021, 143, 19731–19747

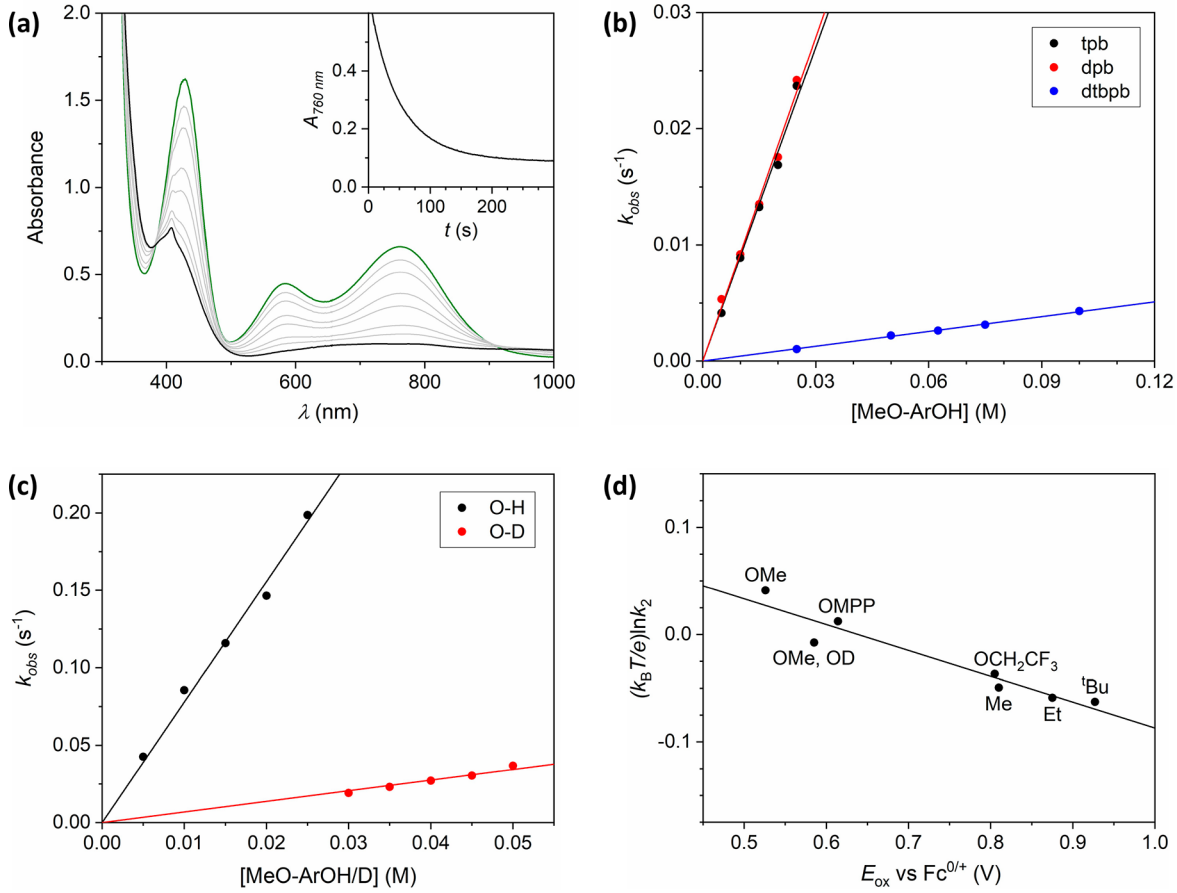

Figure 5. (a) Reaction of $[Cu^{II}(\eta^1\text{-}O_2^{\bullet-})(tpb_3\text{-}TMPA)]^+$ with 4-methoxy-2,6-di-*tert*-butylphenol (MeO-ArOH) in THF solution at −70 °C. Main: UV−vis spectra of the starting complex, product, and those recorded during the course of reaction are depicted using green, black, and gray lines, respectively. Inset: Absorbance at 760 nm as a function of time. (b) Plot of observed rate constants (k_{obs}, s^{-1}) versus substrate concentration (M) for reaction of $[Cu^{II}(\eta^1\text{-}O_2^{\bullet-})(Ar_3\text{-}TMPA)]^+$ (Ar = tpb, dpb, and dtbpb) with MeO-ArOH, in THF solution at −70 °C. (c) Plot of k_{obs} (s^{-1}) versus substrate concentration (M) for reaction of $[Cu^{II}(\eta^1\text{-}O_2^{\bullet-})(tpb_3\text{-}TMPA)]^+$ with MeO-ArOH and MeO-ArOD (black and red circles, respectively) in THF solution at −40 °C. (d) Plot of $(k_BT/e)\ln(k_2)$, obtained from reaction of $[Cu^{II}(\eta^1\text{-}O_2^{\bullet-})(tpb_3\text{-}TMPA)]^+$ with 4-substituted 2,6-di-*tert*-butylphenols (X-ArOH) at −40 °C, versus oxidation potentials (E_{ox} vs Fc^+/Fc^0, V) of the phenol substrates.

end-on binding modes are the ground spin-states of $[Cu^{II}(\eta^1\text{-}O_2^{\bullet-})(Ar_3\text{-}TMPA)]^+$. Similar findings have been reported for a handful of other $Cu^{II}(\eta^1\text{-}O_2^{\bullet-})$ complexes,[33,52−54] which contrasts with the diamagnetic nature of $Cu(\eta^2\text{-}O_2)$ species.[19]

The large aryl substituents of $[Cu^{II}(\eta^1\text{-}O_2^{\bullet-})(Ar_3\text{-}TMPA)]^+$ do not significantly impact the metal−ligand bond lengths in the DFT calculated structures (Figures S31−S33). Indeed, they are essentially identical to those of the corresponding geometry optimized structure of the parent complex $[Cu^{II}(\eta^1\text{-}O_2^{\bullet-})(TMPA)]^+$ (Figure S30). For instance, the Cu−O and O−O bond lengths in $[Cu^{II}(\eta^1\text{-}O_2^{\bullet-})(TMPA)]^+$ and all three $[Cu^{II}(\eta^1\text{-}O_2^{\bullet-})(Ar_3\text{-}TMPA)]^+$ complexes fall within the very narrow ranges of 1.97−1.98 and 1.28−1.29 Å, respectively. Similarly, the Cu−O−O bond angles were calculated to be 116.2−116.9°. All of these values are in excellent agreement with X-ray structural parameters reported for $[Cu^{II}(\eta^1\text{-}O_2^{\bullet-})(TMG_3\text{-}tren)]^+$ (i.e., Cu−O and O−O distances of 1.927(3) and 1.280(3) Å, repectively; Cu−O−O angle of 123.53(18)°).[32] Thus, it can be inferred that any differences in behavior among the $[Cu^{II}(\eta^1\text{-}O_2^{\bullet-})(Ar_3\text{-}TMPA)]^+$ complexes and $[Cu^{II}(\eta^1\text{-}O_2^{\bullet-})(TMPA)]^+$ arise from the differing steric profiles of the ligands.

To better visualize the spatial arrangement of the aryl substituents of the $[Cu^{II}(\eta^1\text{-}O_2^{\bullet-})(Ar_3\text{-}TMPA)]^+$ complexes, topographic steric maps were built from their DFT geometry optimized structures (Figure 4), using the SambVca 2 web tool.[55,56] The conclusions obtained mirror inferences made above, during discussion of the X-ray crystal structures of $[Cu^{II}(Ar_3\text{-}TMPA)(NCMe)]^{2+}$. The planarity of the pyridine donors in $[Cu^{II}(\eta^1\text{-}O_2^{\bullet-})(TMPA)]^+$ leaves ample space for close approach of a second copper center, which allows for facile formation of $[Cu^{II}_2(\mu^2\text{-}O_2^{2-})(TMPA)_2]^{2+}$. The latter has been crystallographically characterized, and one notable feature of its structure is that the pyridine rings of the two separate TMPA ligands interdigitate.[57,58] This is more vividly demonstrated in the crystallographically characterized $Cu^{II}(\mu^2\text{-}O_2^{2-})Cu^{II}$ complex of tris(6-phenylamino)-substitued TMPA, wherein steric bulk projects parallel to the Cu−O axis.[59] In contrast, the aryl substituents of $[Cu^{II}(\eta^1\text{-}O_2^{\bullet-})(Ar_3\text{-}TMPA)]^+$ point away from the metal center, but with much of the steric bulk orientated perpendicular to the plane of the pyridine rings. As such, with the exception of $[Cu^{II}(\eta^1\text{-}O_2^{\bullet-})(dtbpb_3\text{-}TMPA)]^+$, they do not crowd the metal center. Instead, the steric bulk occupies the space between the pyridine donors, thereby prohibiting the interdigitation that is integral to $Cu^{II}(\mu^2\text{-}O_2^{2-})Cu^{II}$ complex formation. Given that projection of steric bulk above the superoxo ligand is minimal (or removed from the center), we contend that this lateral

https://doi.org/10.1021/jacs.1c07837
J. Am. Chem. Soc. 2021, 143, 19731−19747

Table 3. Summary of the Second Order Rate Constants (k_2, M^{-1} s^{-1}) Measured for Reaction of $[Cu^{II}(\eta^1\text{-}O_2^{\bullet-})(tpb_3\text{-}TMPA)]^+$ with Various O−H, N−H, and C−H Bond Substrates in THF Solution at −40 °C and, Where Available, Reported pK_a Values, Oxidation Potentials (E_{ox} vs Fc^+/Fc^0, V), and Bond Dissociation Energies (BDEs, kcal mol^{-1}) of the Substrates

	substrate	k_2 (M^{-1} s^{-1})	BDE (X−H) (kcal mol^{-1})	E_{ox} vs Fc^+/Fc^0 (V)	pK_a
O−H substrates[a]	MeO-ArOH	7.8(4)	79.6	0.526	18.2
	MeO-ArOD	0.69(3)		0.585	
	MPPO-ArOH[b]	1.8(1)		0.614	
	CF_3CH_2O-ArOH	0.16(1)		0.805	
	Me-ArOH	0.086(4)	80.1	0.81	17.7
	Et-ArOH	0.053(3)	80.0	0.875	17.7
	^{t}Bu-ArOH	0.044(2)	82.3	0.927	17.8
N−H substrates[c]	DPH	25(1)	71.7		26.2
	DPH-d_2	1.3(1)			
	TPH	1.3(1)	83.5		24.5
	TPH-d	0.14(1)			
	Ph_2NH	0.00080(4)	89.9	0.455	25.0
C−H substrates[d]	BNAH	0.20(1)	70.7	0.219	
	BzImH	0.0099(5)	73.4	−0.179	

[a]BDE and pK_a values (in DMSO) are taken from ref 60, and the E_{ox} values (in MeCN) are taken from ref 46. [b]MPPO = 2-methyl-1-phenylpropan-2-yloxy. [c]With the exception of the k_2 values, data (measured in DMSO) is taken from ref 67. [d]E_{ox} values and BDEs (in MeCN) are taken from ref 68.

steric bulk is the reason for the high stability of the $[Cu^{II}(\eta^1\text{-}O_2^{\bullet-})(Ar_3\text{-}TMPA)]^+$ complexes.

Quite remarkably, UV−vis spectral features suggestive of trace formation of the complexes $[Cu^{II}(\eta^1\text{-}O_2^{\bullet-})(tpb_3\text{-}TMPA)]^+$ and $[Cu^{II}(\eta^1\text{-}O_2^{\bullet-})(dpb_3\text{-}TMPA)]^+$ are observed even at ambient temperatures (Figure 3b,c and Figures S20 and S21). Consistent with the entropically disfavored nature of O_2 binding, these features increase in intensity at lower temperatures, and by −40 °C formation of the $Cu^{II}(\eta^1\text{-}O_2^{\bullet-})$ species saturates. Reversal of these spectral changes can be achieved by increasing the temperature, which indicates that O_2 binding is reversible. The general oxygenation behavior of $[Cu^{I}(dtbpb_3\text{-}TMPA)]^+$ is similar to that of the tpb- and dpb-substituted systems. However, the onset of formation of $[Cu^{II}(\eta^1\text{-}O_2^{\bullet-})(dtbpb_3\text{-}TMPA)]^+$ occurs at a lower temperature, and it only saturates at ≤−70 °C (Figures 3c and S22). The reduced affinity of $[Cu^{I}(dtbpb_3\text{-}TMPA)]^+$ for O_2 binding is a consequence of the comparative instability of the +2 oxidation state of copper in this system. This is evident from the $E_{1/2}$ value of the $[Cu(Ar_3\text{-}TMPA)(NCMe)]^{2+/+}$ redox couple for Ar = dtbpb, which is 70−90 mV more positive than those of Ar = dpb and tpb (see above).

Crucially, no spectral features associated with formation of higher nuclearity O_2 adducts, including $Cu^{II}(\mu^2\text{-}O_2^{2-})Cu^{II}$ complexes, are observed for any of the $[Cu^{II}(\eta^1\text{-}O_2^{\bullet-})(Ar_3\text{-}TMPA)]^+$ complexes, at any temperature. Furthermore, within a time frame of several hours, no evidence for self-decay of any of these three complexes was observed at temperatures of ≤−20 °C. Above these temperatures, very slow decay does occur, possibly due to reaction with the solvent (or impurities therein), but the final products are presently unclear.

Reaction with Phenolic Substrates. THF was used as the solvent of choice in all of our reactivity studies, and in order to eliminate kinetic complications arising from pre-equilibrium binding of O_2, they were conducted at temperatures at which oxygenation of the $[Cu^{I}(Ar_3\text{-}TMPA)]^+$ complexes display saturation. As mentioned above, for Ar = dtbpb this is ≤−70 °C, whereas higher temperatures of ≤−40 °C are required for Ar = tpb and dpb. The impact of the differing steric profiles of our three $[Cu^{II}(\eta^1\text{-}O_2^{\bullet-})(Ar_3\text{-}TMPA)]^+$ complexes upon reaction with external substrates was, therefore, probed at −70 °C. These studies were performed using 2,6-di-*tert*-butyl-4-methoxyphenol (MeO-ArOH) as a substrate because it has a comparatively weak O−H bond (bond dissociation energy (BDE) = 79.6 kcal mol^{-1})[60] and it is widely used in such studies, thereby allowing comparison with other published systems.

In all cases, addition of excess MeO-ArOH to the $[Cu^{II}(\eta^1\text{-}O_2^{\bullet-})(Ar_3\text{-}TMPA)]^+$ complexes led to first order loss of their chromophores (Figures 5a, S37, and S38). The observed rate constants (k_{obs}) were found to be linearly dependent upon substrate concentration (Figure 5b), thereby yielding the second order rate constants (k_2) listed in Table 2. Near identical k_2 values of 0.90(5) and 0.93(5) M^{-1} s^{-1} were measured for $[Cu^{II}(\eta^1\text{-}O_2^{\bullet-})(tpb_3\text{-}TMPA)]^+$ and $[Cu^{II}(\eta^1\text{-}O_2^{\bullet-})(dpb_3\text{-}TMPA)]^+$, but a more than 20-fold smaller value of 0.042(2) M^{-1} s^{-1} was obtained for $[Cu^{II}(\eta^1\text{-}O_2^{\bullet-})(dtbpb_3\text{-}TMPA)]^+$. Thus, it can be concluded that addition of a phenyl ring to the 4-position of the dpb substituent, to give tpb, has little impact upon reaction with the bulky MeO-ArOH substrate. Considering that these Ph rings point away from the metal center, even if they do increase the steric bulk projecting above the mean plane of the pyridine donor rings (Figure 4c), this is not very surprising. In contrast, the *tert*-butyl groups in the dtbpb substituents might not be expected to impact substrate reactivity significantly because they project laterally. However, it is clear from the topographic steric map in Figure 4d that they crowd the superoxo-occupied axial coordination site, and we believe this is the origin of the suppressed reactivity displayed by this system. Nevertheless, the low reactivity of $[Cu^{II}(\eta^1\text{-}O_2^{\bullet-})(dtbpb_3\text{-}TMPA)]^+$ limits the scope of reactivity studies that can be performed for it. Thus, it was decided that subsequent kinetic studies should focus upon $[Cu^{II}(\eta^1\text{-}O_2^{\bullet-})(tpb_3\text{-}TMPA)]^+$, which has near identical reactivity to $[Cu^{II}(\eta^1\text{-}O_2^{\bullet-})(dpb_3\text{-}TMPA)]^+$ but is easier to synthesize.

Reaction of the three $[Cu^{II}(\eta^1\text{-}O_2^{\bullet-})(Ar_3\text{-}TMPA)]^+$ complexes with MeO-ArOH, at −70 °C, led to formation of similar charge transfer bands centered somewhere around 400−410 nm (Figures 5a, S37, and S38). Concomitantly, formation of

https://doi.org/10.1021/jacs.1c07837
J. Am. Chem. Soc. 2021, 143, 19731−19747

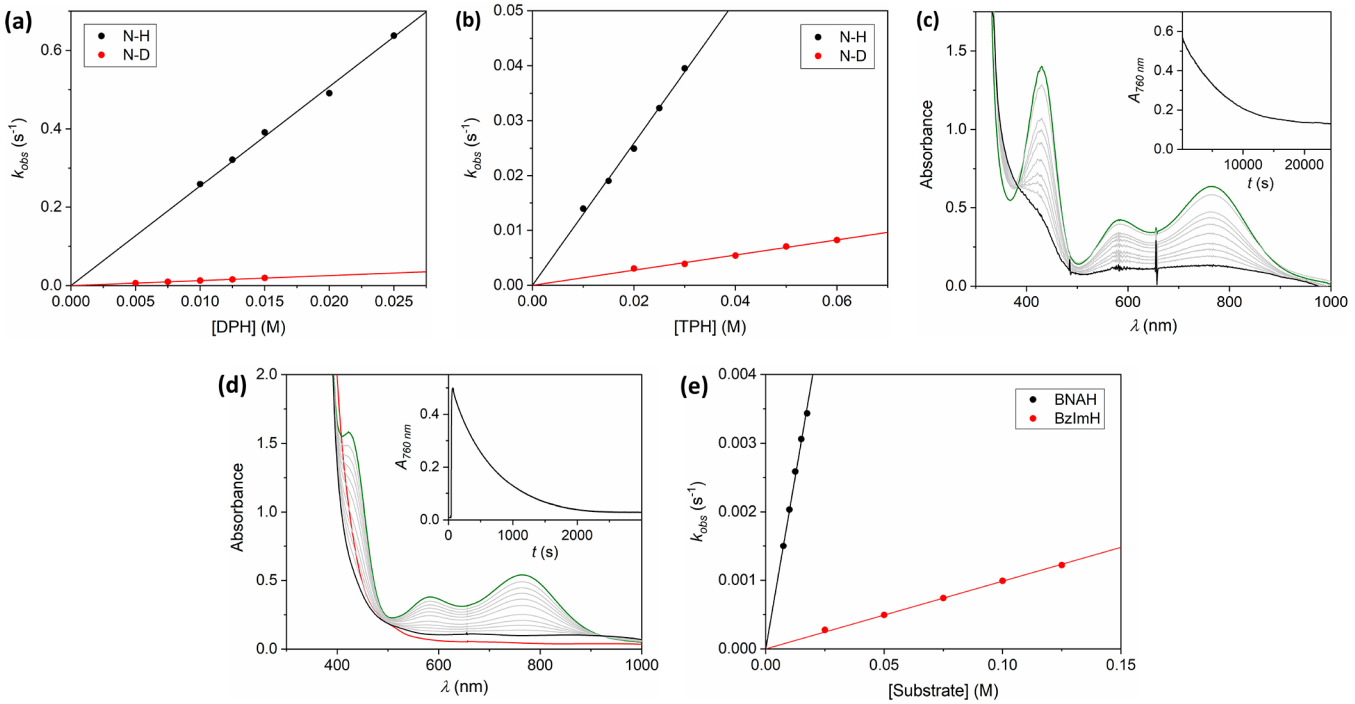

Figure 6. Plots of observed rate constants (k_{obs}, s^{-1}) versus substrate concentration (M) for reaction of $[Cu^{II}(\eta^1\text{-}O_2^{\bullet-})(tpb_3\text{-}TMPA)]^+$ in THF solution at −40 °C, with (a) DPH and its N-deuterated analogue, DPH-d_2 (black and red circles, respectively), and (b) TPH and its N-deuterated analogue, TPH-d (black and red circles, respectively). Reaction of $[Cu^{II}(\eta^1\text{-}O_2^{\bullet-})(tpb_3\text{-}TMPA)]^+$ in THF solution at −40 °C, with the substrates (c) Ph_2NH and (d) BNAH. In the latter case, the substrate was added prior to oxygenation. Main: The starting copper(I) complex (not shown in (c)), superoxocopper(II) intermediate, product of reaction, and the spectra recorded during the course of reaction with the substrate are depicted using red, green, black, and gray lines, respectively. Inset: Absorbance at 760 nm as a function of time. (e) Plot of observed rate constants (k_{obs}, s^{-1}) versus substrate concentration (M) for reaction of $[Cu^{II}(\eta^1\text{-}O_2^{\bullet-})(tpb_3\text{-}TMPA)]^+$ with the C−H bond substrates BNAH and BzImH (black and red circles, respectively), in THF solution at −40 °C.

sharp features at ∼406 nm and bumps at ∼390 nm were observed. These relatively sharp features correspond to the MeO-ArO$^\bullet$ phenoxyl radical.[61] MeO-ArO$^\bullet$ decayed under the reaction conditions employed, so it did not accumulate to high concentrations. Nevertheless, the observation of phenoxyl radicals is indicative of formal transfer of a hydrogen atom to the superoxocopper(II) moiety. From this, it can be inferred that the 400−410 nm charge transfer bands (formed upon reaction with all three $[Cu^{II}(\eta^1\text{-}O_2^{\bullet-})(Ar_3\text{-}TMPA)]^+$) correspond to hydroperoxocopper(II) complexes, $[Cu^{II}(OOH)(Ar_3\text{-}TMPA)]^+$. Good agreement of their UV−vis and EPR (Figure S34) spectral features with those of previously reported hydroperoxocopper(II) complexes support this supposition.[23,48,62−66] Furthermore, similar species could be obtained by addition of the H atom donor TEMPO-H to $[Cu^{II}(\eta^1\text{-}O_2^{\bullet-})(tpb_3\text{-}TMPA)]^+$ (Figure S39) and by treatment of $[Cu^{II}(tpb_3\text{-}TMPA)(NCMe)]^{2+}$ with a combination of H_2O_2 and NEt_3 (Figure S40), both of which are standard methods for preparation of hydroperoxocopper(II) complexes.

The observed phenoxyl radical and $[Cu^{II}(OOH)(Ar_3\text{-}TMPA)]^+$ products can be obtained either through a hydrogen atom transfer (HAT) reaction or (in either order) a stepwise transfer of a proton and an electron (i.e., PT-ET or ET-PT). To probe these mechanistic possibilities, we sought to expand the range of phenolic substrates studied. However, the k_2 value measured for reaction of $[Cu^{II}(\eta^1\text{-}O_2^{\bullet-})(tpb_3\text{-}TMPA)]^+$ with MeO-ArOH, at −70 °C, is (after taking temperature into account) 1−2 orders of magnitude smaller than those reported for the analogous reaction with other TMPA-supported $Cu^{II}(\eta^1\text{-}O_2^{\bullet-})$ complexes (Table S10). Such sluggish reaction renders measurement of reaction kinetics with more oxidatively resistant phenols challenging at this temperature. Fortunately, the high stability of $[Cu^{II}(\eta^1\text{-}O_2^{\bullet-})(tpb_3\text{-}TMPA)]^+$ allows mitigation of this problem via study at higher temperatures.

The kinetic isotope effect (KIE) upon reaction of $[Cu^{II}(\eta^1\text{-}O_2^{\bullet-})(tpb_3\text{-}TMPA)]^+$ with MeO-ArOH was measured at −40 °C. At this temperature, k_2 values of 7.8(4) and 0.69(3) M^{-1} s^{-1} were obtained for MeO-ArOH and its isotopomer MeO-ArOD (Figure 5c, Table 3), respectively, which equate to a KIE of 11.3(8). This confirms that the rate-determining step involves HAT or a proton transfer (PT). Similar KIEs were reported for reaction of $[Cu^{II}(\eta^1\text{-}O_2^{\bullet-})(DMM\text{-}TMPA)]^+$ with the same substrate (11)[46] and for reaction of the active oxidants of the enzymes PHM, DβM, and TβM (10−12), which are evidenced to be $Cu^{II}(\eta^1\text{-}O_2^{\bullet-})$ intermediates.[11,13,14] These published values were all presented as supporting evidence for HAT mechanisms.

In addition, we measured kinetics at −40 °C for reaction of $[Cu^{II}(\eta^1\text{-}O_2^{\bullet-})(tpb_3\text{-}TMPA)]^+$ with several 2,6-di-*tert*-butylphenols possessing differing substituents (X) at the 4-position (X-ArOH, Scheme S4). Reaction was found, in all cases, to proceed with a first order dependence upon both complex and substrate, thereby yielding second order rate constants (Figures S41). The k_2 values obtained are summarized alongside reported BDE, E_{ox}, and pK_a values, where available, in Table 3. The organic products of the reactions of $[Cu^{II}(\eta^1\text{-}O_2^{\bullet-})(tpb_3\text{-}TMPA)]^+$ with the X-ArOH substrates at −40 °C were characterized upon warming to room temperature, and in all cases, approximately 0.5 equiv of 2,6-di-*tert*-butyl-1,4-

https://doi.org/10.1021/jacs.1c07837
J. Am. Chem. Soc. 2021, 143, 19731−19747

Scheme 2. Summary of the Substrates Used in Reaction Kinetics Studies of $[Cu^{II}(\eta^1\text{-}O_2^{\bullet-})(tpb_3\text{-}TMPA)]^+$ and the Organic Products Formed[a]

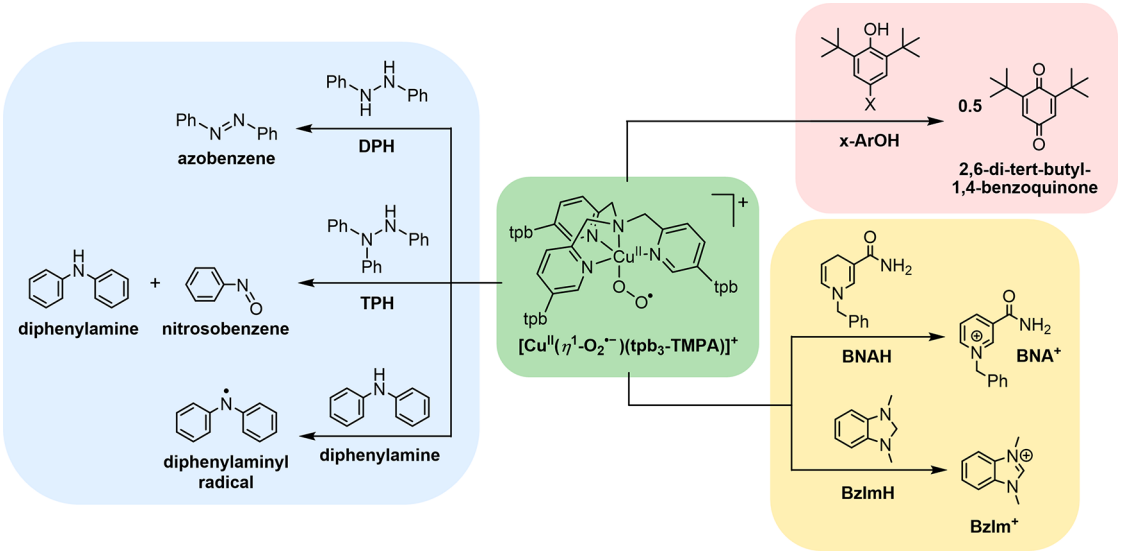

[a]In X-ArOH, X = OMe, MPPO, OCH_2CF_3, Me, Et, and ^{t}Bu. MPPO = 2-methyl-1-phenylpropan-2-yloxy.

benzoquinone was obtained. This outcome has precedence, and a mechanism explaining it, via initial generation of phenoxyl radicals, has been provided elsewhere.[46]

A Marcus-type plot of $(k_BT/e)\ln(k_2)$ versus oxidation potential (E_{ox}) of the phenols was constructed from the data obtained (Figure 5d).[30] It displays a good linear correlation, with a best-fit line possessing a slope of −0.24. The observation of a negative slope rules out a mechanism involving an initial discrete PT step. This is because the rate of a PT reaction would be expected to increase with decreasing pK_a, and given that the pK_a of phenols is inversely related to their E_{ox} values, a positive slope should result. The magnitude of the slope observed for $[Cu^{II}(\eta^1\text{-}O_2^{\bullet-})(tpb_3\text{-}TMPA)]^+$ is much larger than that reported for the cumylperoxyl radical (−0.05),[46,69] which is accepted to react with phenols and (*N*,*N*-dimethylanilines) via "pure" HAT.[69,70] However, it is smaller than expected for a reaction involving an initial electron transfer and subsequent separate proton transfer step (−0.5 to −1.0).[69,71,72] Instead, the observed correlation and slope are suggestive of a HAT reaction in which there is significant charge (electron) transfer.[73,74] A similar observation was reported for $[Cu^{II}(\eta^1\text{-}O_2^{\bullet-})(DMA\text{-}TMPA)]^+$, but a linear fit with a slightly larger gradient of −0.29 was obtained.[46] From this, it can be cautiously inferred that reaction of $[Cu^{II}(\eta^1\text{-}O_2^{\bullet-})(DMA\text{-}TMPA)]^+$ with phenols proceeds with greater charge transfer than $[Cu^{II}(\eta^1\text{-}O_2^{\bullet-})(tpb_3\text{-}TMPA)]^+$. One might expect this to manifest in differences in enthalpic barriers to reaction of these two complexes.

To further probe the oxidative potency of $[Cu^{II}(\eta^1\text{-}O_2^{\bullet-})(tpb_3\text{-}TMPA)]^+$, it was combined with the electron transfer agents ferrocene and decamethylferrocene (0.00 and −0.48 V, respectively, in MeCN solution).[75] No reaction was observed in either case. This contrasts with $[Cu^{II}(\eta^1\text{-}O_2^{\bullet-})(L8)]^+$, which is able to react with both.[41] It is also worth mentioning that although reaction was observed upon addition of 2,6-di-*tert*-butylphenol (H-ArOH), it was so slow that no attempts were made to measure reaction kinetics. This reflects the higher E_{ox} of this phenol (1.074 V) relative to the other X-ArOH substrates.[46] Given that H-ArOH also has a lower pK_a (17.3)[60] than the other X-ArOH substrates, it reinforces the inference that $[Cu^{II}(\eta^1\text{-}O_2^{\bullet-})(tpb_3\text{-}TMPA)]^+$ is also a comparatively weak base. These negative results reaffirm the conclusion that HAT is the mechanism by which this complex reacts with phenols.

Reaction with N−H and C−H Substrates. In order to obtain a broader understanding of the reactivity of the $[Cu^{II}(\eta^1\text{-}O_2^{\bullet-})(Ar_3\text{-}TMPA)]^+$ complexes, we expanded our studies (at −40 °C) to include N−H and C−H bond substrates. As with the phenolic substrates, reaction was found in all cases to be first order in both substrate and $Cu^{II}(\eta^1\text{-}O_2^{\bullet-})$ complex (i.e., second order overall). Consistent with their respective relatively low BDEs of 71.7 and 83.5 kcal mol^{-1},[67] the substrates 1,2-diphenylhydrazine (DPH) and 1,1,2-triphenylhydrazine (TPH) are rapidly oxidized by $[Cu^{II}(\eta^1\text{-}O_2^{\bullet-})(tpb_3\text{-}TMPA)]^+$ (Figures 6a,b S42, and S43). More specifically, k_2 values of 25(1) and 1.3(1) M^{-1} s^{-1} were measured for reaction with DPH and TPH, respectively. Subsequent room temperature workup and analysis of the reaction mixtures confirmed that both substrates were oxidized by 2e$^-$ to give ∼1 equiv of product(s). In the case of DPH, this afforded azobenzene in 101(5)% yield (Scheme 2, Table S7). However, oxidation of TPH proceeded via N−N bond cleavage and yielded nitrosobenzene and diphenylamine in yields of 108(9)% and 113(9)% (Scheme 2, Tables S8 and S9), respectively. EPR spectroscopic analysis of the product mixtures from reaction with DPH and TPH, prior to workup, yielded spectra containing a single copper(II)-containing species (Figure S35). This was the only EPR-active species produced from reaction with DPH, but an intense signal indicative of an organic radical was obtained upon oxidation of TPH. For reasons explained below, this is believed to be $Ph_2N^{\bullet}$.

Reaction with the corresponding N-deuterated hydrazines DPH-d_2 and TPH-d proceeded with significantly reduced k_2 values (Figure 6a,b) of 1.3(1) and 0.14(1) M^{-1} s^{-1}, respectively. This equates to substantial KIEs of 19.8(14) for DPH and 9.4(7) for TPH. These values are comparable to (or larger than) those obtained from reaction with MeO-ArOH.

https://doi.org/10.1021/jacs.1c07837
J. Am. Chem. Soc. 2021, 143, 19731−19747

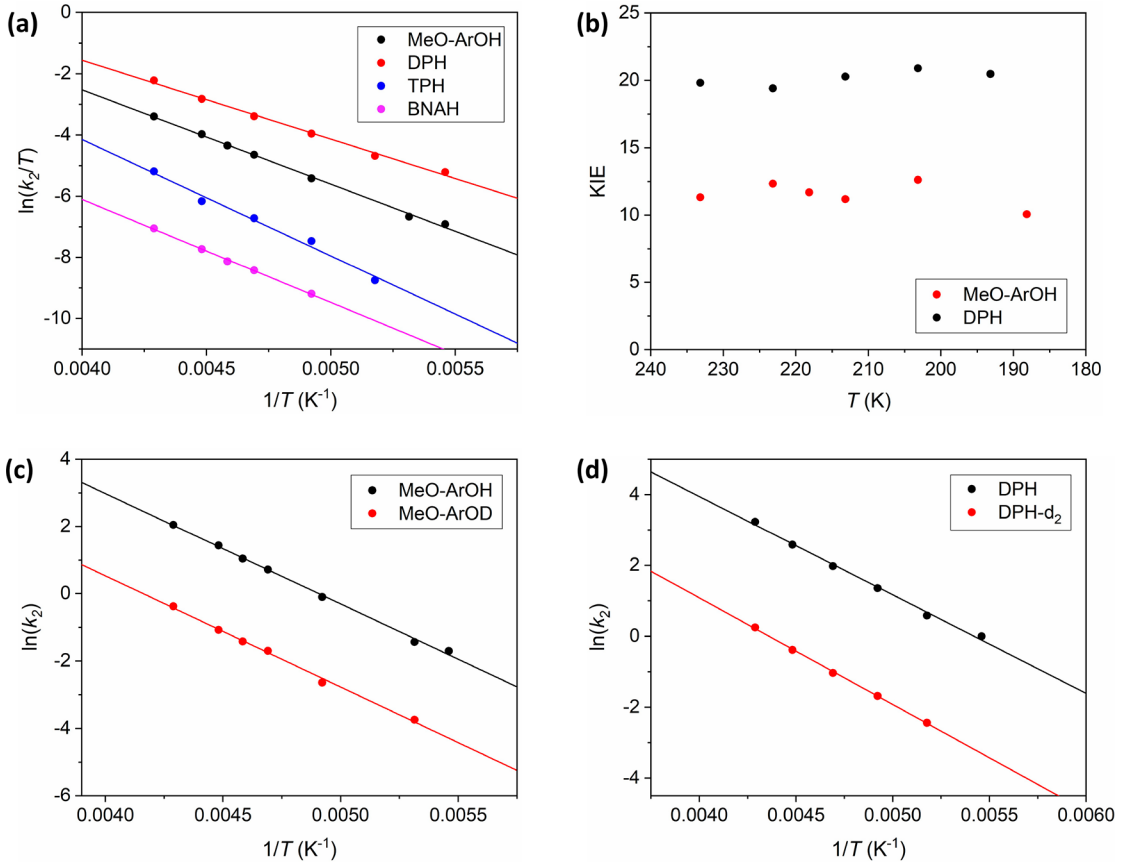

Figure 7. (a) Eyring plots for reaction of $[Cu^{II}(\eta^1\text{-}O_2^{\bullet-})(tpb_3\text{-}TMPA)]^+$ with the substrates MeO-ArOH, DPH, TPH, and BNAH (black, red, blue, and magenta circles, respectively). (b) Kinetic isotope effects (KIEs) upon reaction of $[Cu^{II}(\eta^1\text{-}O_2^{\bullet-})(tpb_3\text{-}TMPA)]^+$ with MeO-ArOH and DPH (red and black circles, respectively) versus temperature (T, K). The KIE values used to construct the plot are listed in Tables S11 and S12. Arrhenius plots for reaction of $[Cu^{II}(\eta^1\text{-}O_2^{\bullet-})(tpb_3\text{-}TMPA)]^+$ with (c) MeO-ArOH and MeO-ArOD (black and red circles, respectively) and (d) DPH and DPH-d_2 (black and red circles, respectively). Plots of k_{obs} versus substrate concentration, as a function of temperature, used to construct (a)−(d) appear in the Supporting Information (Figures S47−S52). The second order constants derived therefrom are listed in Tables S11−S14, and the values obtained from fitting the Arrhenius plots are listed in Table S15.

Given that hydrazines are less acidic than phenols, these large KIEs can be attributed to HAT reactivity. In fact, the KIE for reaction with DPH is sufficiently large to imply H atom tunneling contributions.

In addition to hydrazines, we attempted reaction with the more challenging substrate diphenylamine (Ph_2NH), which possesses a relatively high N−H BDE of 89.9 kcal mol^{-1}.[67] It was successful, albeit very slow, and proceeded with a k_2 value of 8.0(4) × 10^{-4} M^{-1} s^{-1} (Figures 6c and S44). The success of the reaction was confirmed by study of the crude reaction mixture by EPR spectroscopy (Figure S35). In addition to a copper-containing species, a signal characteristic of an organic radical was observed. Considering that an identical organic radical was also observed upon oxidation of TPH, which yields Ph_2NH as a product, this is assumed to be $Ph_2N^{\bullet}$. The E_{ox} of diphenylamine (0.455 V) is much higher than that of decamethylferrocene, and its pK_a (25.0) is significantly higher than the 4-substituted-2,6-di-*tert*-butylphenols used in this study. Thus, reaction via an initial H^+ or e^- transfer can be ruled out and, instead, oxidation most likely occurs by HAT.

Oxidation of C−H bond substrates proved to be a more challenging proposition. One difficulty arose from the coordinating nature of the olefinic functional groups present in many substrates containing activated C−H bonds. This allows them to compete with O_2 in binding to the copper(I) starting complex $[Cu^{I}(tpb_3\text{-}TMPA)]^+$. Consequently, addition of such substrates to $[Cu^{II}(\eta^1\text{-}O_2^{\bullet-})(tpb_3\text{-}TMPA)]^+$ causes an initial drop in the concentration of this complex due to partial reversal of O_2 binding and formation of $[Cu^{I}(tpb_3\text{-}TMPA)(olefin)]^+$ complexes. This is graphically demonstrated by sequential addition of multiple portions of 1,4-cyclohexadiene (CHD) to $[Cu^{II}(\eta^1\text{-}O_2^{\bullet-})(tpb_3\text{-}TMPA)]^+$ (Figure S45). Oxidation of this substrate is extremely sluggish, and the CHD portions only cause stepwise incremental decreases in $Cu^{II}(\eta^1\text{-}O_2^{\bullet-})$ concentration. Although this ligand metathesis process is much more rapid than substrate oxidation for the C−H bond substrates studied, it does complicate simulation of reaction kinetics. Thankfully, this problem can be circumvented by adding substrate to the copper(I) starting complex prior to oxygenation, which results in a clean first order reaction with $[Cu^{II}(\eta^1\text{-}O_2^{\bullet-})(tpb_3\text{-}TMPA)]^+$ (Figures 6d and S46).

Reaction with 1-benzyl-1,4-dihydronicotinamide (BNAH) and 1,3-dimethyl-2,3-dihydrobenzimidazole (BzImH), which have very low C−H BDEs of 70.7 and 73.4 kcal mol^{-1},[68] afforded ∼1 equiv of their 2e$^-$ oxidized products 1-benzylnicotinamidium (BNA^+) and 1,3-dimethylbenzimidazolium ($BzIm^+$) after workup (Scheme 2, Tables S5 and S6). Interestingly, EPR spectra of the product mixtures, prior to workup, possess relatively poor signal intensity in the case of

https://doi.org/10.1021/jacs.1c07837
J. Am. Chem. Soc. 2021, 143, 19731−19747

Table 4. Activation Enthalpies and Entropies ($\Delta H^{\ddagger}$ and $\Delta S^{\ddagger}$, Respectively) Obtained from Eyring Plots and Parameters Calculated from Arrhenius Analysis of Temperature Dependent KIE Measurements (ΔE_A and A_H/A_D) for Reaction of $[Cu^{II}(\eta^1\text{-}O_2^{\bullet-})(tpb_3\text{-}TMPA)]^+$ and Selected Complexes with Substrates[a]

complex	substrate	$\Delta H^{\ddagger}$ (kcal mol^{-1})	$\Delta S^{\ddagger}$ (cal mol^{-1} K^{-1})	ΔE_A (kcal mol^{-1})	A_H/A_D
$[Cu^{II}(\eta^1\text{-}O_2^{\bullet-})(tpb_3\text{-}TMPA)]^+$	MeO-ArOH	6.1 ± 0.1	−28 ± 0.6	0.034	11
	DPH	5.1 ± 0.2	−30 ± 0.9	0.45	7.1
	TPH	7.6 ± 0.5	−25 ± 2.4		
	BNAH	6.7 ± 0.2	−33 ± 0.7		
$[Cu^{II}(\eta^1\text{-}O_2^{\bullet-})(DMM\text{-}TMPA)]^+$ [46]	MeO-ArOH	3.6 ± 0.6	−32 ± 3		
$[Cu^{II}(\eta^1\text{-}O_2^{\bullet-})(L8)]^+$ [43]	benzylic CH_2	4.5 ± 0.02	−53 ± 0.1		
$Cu^{II}(1,2\text{-}\mu\text{-}O_2^{\bullet-})Cu^{II}$ [83]	TEMPO-H	9.0 ± 0.4	−27 ± 1.7		
$[Cu^{III}(OH)(L)]^-$ [84,85]	DHA	5.1(1)	−31(3)	0.3	13
$[Cu^{III}(OH)(^{NO2}L)]^-$ [84]	DHA	4.9(1)	−27(1)	3.0	0.05
$[Cu^{III}(OH)(^{pipMe}L)]^-$ [84]	DHA	3.8(2)	−38(3)	3.6	0.01
$[Co^{III}(\eta^1\text{-}O_2^{\bullet-})(py)(TBP_8Cz)]^-$ [86]	DPH	6.7 ± 0.1	−23 ± 0.4		
$[Cr^{III}(\eta^1\text{-}O_2^{\bullet-})(Cl)(TMC)]^+$ [87]	$AcrH_2$			10.8	4.1×10^{-8}
PHM[15]	hippuric acid			0.37	5.9
WT-SLO[88]	linoleic acid			0.9	18

[a] $\Delta E_A = E_a(H) - E_a(D)$, which is the difference between the activation energies for reaction with protio substrates and their deuterated congeners and A_H/A_D is the ratio of the associated collision frequencies.

BNAH and next to no signal for BzImH (Figure S36). The latter, in particular, is consistent with the formation of copper(I)-containing products. Efforts to identify these species have been unsuccessful thus far but are ongoing.

In addition to being H atom donors, BNAH and BzImH are also potential hydride donors. However, their relative tendencies to function as hydride donors (64.2 kcal mol^{-1} for BNAH and 49.5 kcal mol^{-1} for BzImH)[68] are the reverse of their H atom donor abilities. More specifically, BNAH is more reactive than BzImH as a H atom donor but weaker as a H$^-$ donor. Given that $[Cu^{II}(\eta^1\text{-}O_2^{\bullet-})(tpb_3\text{-}TMPA)]^+$ reacts with BNAH 20 times more quickly than with BzImH (Figure 6e, k_2 values of 0.20(1) and 0.0099(5) M^{-1} s^{-1}, respectively), it can be concluded that reaction proceeds via HAT. This outcome mirrors that previously reported for $[Cu^{II}(\eta^1\text{-}O_2^{\bullet-})(^{(Piv)}TMPA)]^+$, which reacts 2.4 times more quickly with BNAH than it does with BzImH.[47]

The rates measured for reaction of $[Cu^{II}(\eta^1\text{-}O_2^{\bullet-})(tpb_3\text{-}TMPA)]^+$ with BNAH and BzImH are significantly lower than those measured for reaction with MeO-ArOH and TPH, despite the latter substrates possessing O−H and N−H bonds that are significantly stronger than the C−H bonds of the former (Table 3). Indeed, attempts to measure reaction kinetics for the substrates xanthene and 9,10-dihydroanthracene, which have slightly higher C−H BDEs (77.9 and 80.6 kcal mol^{-1}, respectively)[67] were unsuccessful, with no kinetically measurable reaction being observed at −40 °C. This implies that factors beyond simple thermodynamic considerations are important in controlling reactivity.

It has long been known that HAA from C−H bonds is very slow relative to HAA from O−H and N−H bonds.[76,77] This has been rationalized using the Marcus cross relation:[78−80]

$$k_{AH/B} = \sqrt{k_{AH/A} k_{BH/B} K_{eq} f}$$

where K_{eq} is the equilibrium constant for the HAT in question, which equates to the thermodynamic driving force for the reaction, $k_{AH/A}$ and $k_{BH/B}$ are H atom self-exchange rate constants, and f is the frequency factor, which is usually assumed to be close to 1.[81] In our case, $k_{AH/A}$ is associated with self-exchange between $[Cu^{II}(\eta^1\text{-}O_2^{\bullet-})(tpb_3\text{-}TMPA)]^+$ and the corresponding $Cu^{II}(\eta^1\text{-}OOH)$ complex, and $k_{BH/B}$ is for the reacting bond of the substrate (X−H) and the immediate product of HAA (X$^{\bullet}$). For reactions of $[Cu^{II}(\eta^1\text{-}O_2^{\bullet-})(tpb_3\text{-}TMPA)]^+$ with C−H and N/O−H bonds possessing identical BDFEs (i.e., identical K_{eq} values), the rate is dependent upon the respective $k_{BH/B}$ values of the substrates. Rates of self-exchange for C−H bond substrates tend to be several orders of magnitude smaller than those for O−H and N−H bonds.[80,82] Thus, reaction with C−H bonds is expected and experimentally observed to be inherently slower.

Activation Parameters. The high stability of $[Cu^{II}(\eta^1\text{-}O_2^{\bullet-})(tpb_3\text{-}TMPA)]^+$ against formation of higher nuclearity species allows for measurement of kinetic data over a broad temperature range, which provides an opportunity to access more detailed mechanistic information. To exploit this, we have measured k_2 values for reaction with selected substrates at regular increments over temperature ranges of −40 to −90 °C (Figures S47−S52, Tables S11−S14). Given how sluggish reaction is at lower temperatures, these studies are limited to the easily oxidized substrates MeO-ArOH, DPH, TPH, and BNAH. Linear fits of the Eyring plots constructed using these data (Figure 7a) provided the enthalpic ($\Delta H^{\ddagger}$) and entropic ($\Delta S^{\ddagger}$) barriers to reaction listed in Table 4.

The most prominent feature of the activation parameters measured for reaction of $[Cu^{II}(\eta^1\text{-}O_2^{\bullet-})(tpb_3\text{-}TMPA)]^+$ with the substrates MeO-ArOH, DPH, TPH, and BNAH are the large entropic barriers to reaction. This is characteristic of (bimolecular) HAT reactions and reflects the highly preorganized nature of their transition states. The $\Delta S^{\ddagger}$ measured for reaction with BNAH, of −33 ± 0.7 cal mol^{-1} K^{-1}, is the largest among the substrates studied. However, the entropic barriers for reaction with the other substrates are not enormously different, and the sluggish reaction with BNAH is also contributed to by a comparatively large $\Delta H^{\ddagger}$ of 6.7 ± 0.2 kcal mol^{-1}.

Thus far, few measurements have been made of Eyring parameters for HAT reactions between $Cu^{II}(\eta^1\text{-}O_2^{\bullet-})$ complexes and substrates. One of the few reports is for reaction of $[Cu^{II}(\eta^1\text{-}O_2^{\bullet-})(DMA\text{-}TMPA)]^+$ with MeO-ArOH, where $\Delta H^{\ddagger}$ and $\Delta S^{\ddagger}$ values of 3.6 ± 0.6 kcal mol^{-1} and −32 ± 3 cal mol^{-1} K^{-1} were obtained.[46] Another example is reaction of Meyer's pyrazolate-bridged $Cu^{II}(\eta^1\text{-}O_2^{\bullet-})Cu^{II}$ complex with

https://doi.org/10.1021/jacs.1c07837
J. Am. Chem. Soc. 2021, 143, 19731−19747

TEMPO-H, which was accompanied by $\Delta H^{\ddagger}$ and $\Delta S^{\ddagger}$ values of 9.0 ± 0.4 kcal mol^{-1} and −26.8 ± 1.7 cal mol^{-1} K^{-1}, respectively.[83] The $\Delta S^{\ddagger}$ values for the two aforementioned systems are quite similar to that measured for reaction of $[Cu^{II}(\eta^1\text{-}O_2^{\bullet-})(tpb_3\text{-}TMPA)]^+$ with MeO-ArOH (−28 ± 0.6 cal mol^{-1} K^{-1}). Instead, the major difference between the activation parameters for these three reactions with O−H bonds is the magnitude of their respective $\Delta H^{\ddagger}$ values. The most reactive system, $[Cu^{II}(\eta^1\text{-}O_2^{\bullet-})(DMA\text{-}TMPA)]^+$, has the lowest enthalpic barrier to reaction, and the least reactive, the $Cu^{II}(\eta^1\text{-}O_2^{\bullet-})Cu^{II}$ complex, has the largest. The $\Delta H^{\ddagger}$ of 6.1 ± 0.1 kcal mol^{-1} measured for $[Cu^{II}(\eta^1\text{-}O_2^{\bullet-})(tpb_3\text{-}TMPA)]^+$ is intermediate in size. Although other factors may contribute, it is likely that the differences in reactivity of these superoxocopper(II) complexes are correlated with their relative thermodynamic driving forces for reaction (i.e., the strength of the Cu^{II}OO-H bonds formed). This may be related to our above suggestion of greater charge transfer in the HAT reactivity of $[Cu^{II}(\eta^1\text{-}O_2^{\bullet-})(DMM\text{-}TMPA)]^+$ with X-ArOH substrates compared to $[Cu^{II}(\eta^1\text{-}O_2^{\bullet-})(tpb_3\text{-}TMPA)]^+$.

Eyring parameters have been reported for reaction of the superoxocobalt(III) complex $[Co^{III}(\eta^1\text{-}O_2^{\bullet-})(py)(TBP_8Cz)]^-$ with DPH. These $\Delta H^{\ddagger}$ and $\Delta S^{\ddagger}$ values, of 6.7 ± 0.1 kcal mol^{-1} and −23 ± 0.4 cal mol^{-1} K^{-1},[86] are respectively larger and smaller than those measured for $[Cu^{II}(\eta^1\text{-}O_2^{\bullet-})(tpb_3\text{-}TMPA)]^+$ (5.1 ± 0.2 kcal mol^{-1} and −30 ± 0.9 cal mol^{-1} K^{-1}, respectively). Within the temperature window of study, these two factors counterbalance each other, and the two complexes display similar rates of reaction. TPH has a stronger N−H bond than DPH, and as a consequence, the enthalpic barrier to reaction of the former substrate with $[Cu^{II}(\eta^1\text{-}O_2^{\bullet-})(tpb_3\text{-}TMPA)]^+$ is significantly larger (7.6 ± 0.5 kcal mol^{-1}) and reaction is slower.

Concordant with the kinetically inert nature of C−H bonds, there are very few reports of activation parameters for reaction of C−H bond substrates with $Cu^{II}(\eta^1\text{-}O_2^{\bullet-})$ complexes. Indeed, the values reported for intramolecular self-hydroxylation of $[Cu^{II}(\eta^1\text{-}O_2^{\bullet-})(L8)]^+$ represent the best point of comparison for those obtained from reaction of $[Cu^{II}(\eta^1\text{-}O_2^{\bullet-})(tpb_3\text{-}TMPA)]^+$ with BNAH. The entropic barrier to self-hydroxylation in the former is very large (−53 ± 0.1 cal mol^{-1} K^{-1}), much larger than the latter, intermolecular reaction (−33 ± 0.7 cal mol^{-1} K^{-1}). This implies that the transition state for self-decay of $[Cu^{II}(\eta^1\text{-}O_2^{\bullet-})(L8)]^+$ has particularly severe geometric constraints. Without knowing the thermodynamic driving forces for these reactions, further insight is difficult. Correspondingly, it is difficult to make direct comparisons with other complexes when different substrates have been employed, such as Tolman's hydroxocopper(III) complexes, whose activation parameters vary quite significantly upon modification of the supporting ligand. To allow more meaningful conclusions to be drawn, a much larger survey of Eyring parameters for reaction of $Cu^{II}(\eta^1\text{-}O_2^{\bullet-})$ complexes with substrates is required.

Temperature Dependence of KIEs. Kinetic isotope effect (KIE) measurements can be highly informative and allow inferences to be drawn about reaction mechanism. For instance, HAT reactions are frequently marked by large KIE values, with H atom tunneling being suggested for values that far exceed semiclassical limits. However, assessment on this basis alone can sometimes lead to incorrect elimination of tunneling as a mechanism, and it has been shown that more robust information can be obtained from temperature-dependent KIE measurements and the Arrhenius parameters derived therefrom.[89−91] More specifically, from the ratio of the collision factors for reaction with the protio and deuterio substrates (A_H/A_D) and differences in the associated activation energies ($\Delta E_a = E_a(H) - E_a(D)$). Such variable temperature KIE studies have proven to be very revealing in enzymatic studies. However, they are seldom performed for model complexes and other than inconclusive measurements for $[Cu^{II}(\eta^1\text{-}O_2^{\bullet-})(DMA\text{-}TMPA)]^+$ (due to the very limited temperature range studied),[46] we are unaware of any examples for superoxocopper(II) model complexes.

For a semiclassical HAT reaction, A_H/A_D should equal 1 ($\Delta E_a > 0$), with KIE values arising from differences in zero-point energies. Models with corrections for H atom tunneling through the reaction barrier are characterized by $A_H/A_D < 1$ and $\Delta E_a \gg 0$. This can give rise to highly temperature sensitive KIEs, with very large values often being seen at low temperatures. Reaction of the complexes $[Cu^{III}(OH)(^{NO2}L)]^-$ and $[Cu^{III}(OH)(^{pipMe}L)]^-$ with DHA, reported by Tolman and co-workers,[84] and reaction of $[Cr^{III}(\eta^1\text{-}O_2^{\bullet-})(Cl)(TMC)]^+$ with $AcrH_2$, reported by Nam and co-workers,[87,92] both adhere to this paradigm. In particular, the latter proceeds with a KIE of 74 ± 5 at −20 °C that increases to a remarkably large value of 470 ± 30 at −40 °C.[87] Correspondingly, the ΔE_a of 10.8 kcal mol^{-1} and A_H/A_D of only 4.1 × 10^{-8} measured for this system deviate greatly from semiclassical values.

A third scenario involving extensive tunneling of both H and D atoms yields temperature independent KIE values, which equate to $A_H/A_D > 1$ and near-zero ΔE_a values. This type of behavior has been observed at physiological temperatures in wild-type enzymes, where HAT donor−acceptor distances can be optimized by the secondary structure of the enzyme active site. For example, in peptidylglycine α-amidating monoxygenase and soybean lipoxygenase (A_H/A_D = 5.9 and 18, respectively),[15,88] wherein their respective end-on superoxocopper(II) and hydroxoiron(III) active oxidants are responsible for substrate C−H bond oxidation. However, model complexes tend to show this type of behavior only at low temperatures. For example, reaction of Tolman's hydroxocopper(III) complex $[Cu^{III}(OH)(L)]^-$ with DHA (from −20 to −80 °C) is accompanied by a large A_H/A_D of 13 and a ΔE_a of only 0.3 kcal mol^{-1}.[84,85] This diverges significantly from the temperature dependence of the KIEs measured for its derivatives $[Cu^{III}(OH)(^{NO2}L)]^-$ and $[Cu^{III}(OH)(^{pipMe}L)]^-$.

For $[Cu^{II}(\eta^1\text{-}O_2^{\bullet-})(tpb_3\text{-}TMPA)]^+$, KIE measurements over a reasonably large temperature range are only feasible for the most reactive substrates, MeO-ArOH and DPH. In both cases, the KIE values are essentially temperature independent between −40 and −90 °C (Figure 7b), with those of MeO-ArOH and DPH falling within the ranges 10.1(7)−12.6(9) and 19.4(14)−20.9(15), respectively. This is readily apparent from the quasi-parallel nature of the best fit lines in the Arrhenius plots constructed for the substrates MeO-ArOH and MeO-ArOD (Figure 7c), and DPH and DPH-d_2 (Figure 7d). The ΔE_a and A_H/A_D values derived from these plots are listed in Table 4. Consistent with the preceding assertions, respective ΔE_a and A_H/A_D values of 0.034 kcal mol^{-1} and 11 were obtained for MeO-ArOH and MeO-ArOD. Corresponding values of 0.45 kcal mol^{-1} and 7.1 were obtained for DPH and DPH-d_2. On this basis, we can conclude that the HAT reactions between $[Cu^{II}(\eta^1\text{-}O_2^{\bullet-})(tpb_3\text{-}TMPA)]^+$ and these

https://doi.org/10.1021/jacs.1c07837
J. Am. Chem. Soc. 2021, 143, 19731−19747

substrates, which possess weak O−H and N−H bonds, proceed via tunneling of both H and D atoms.

CONCLUSION

In this study, we have shown that installation of bulky aryl substituents at the 5-position of the pyridyl rings of the TMPA ligand provides copper(I) complexes, $[Cu^{I}(Ar_3\text{-TMPA})]^{+}$ (Ar = tpb, dph, dtbpb), that undergo reversible oxygenation to yield the corresponding $[Cu^{II}(\eta^1\text{-}O_2^{\bullet-})(Ar_3\text{-TMPA})]^{+}$ complexes, which possess $S = 1$ ground spin-states. Crucially, no conversion to higher nuclearity species, such as $Cu^{II}(\mu^2\text{-}O_2^{2-})Cu^{II}$ complexes, was observed under any of the experimental conditions studied. As can be seen from X-ray crystal structures of $[Cu^{II}(Ar_3\text{-TMPA})(NCMe)]^{2+}$ and topographic steric maps of $[Cu^{II}(\eta^1\text{-}O_2^{\bullet-})(Ar_3\text{-TMPA})]^{+}$, derived from DFT calculated structures, the aryl substituents point away from the metal center and the majority of their bulk projects perpendicular to the plane of the pyridine rings. This lateral bulk fills the space between the pyridine donors and prohibits their interdigitation, which is a prerequisite of dinuclear complex formation.

Consistent with its entropically disfavored nature, the extent of O_2 binding increases with decreasing temperature, and it can be reversed by warming to ambient temperatures. Oxygenation for Ar = tpb and dpb saturates by −40 °C and traces of their $[Cu^{II}(\eta^1\text{-}O_2^{\bullet-})(Ar_3\text{-TMPA})]^{+}$ complexes can even be observed at room temperature. However, lower temperatures of ∼0 °C are required for commencement of O_2 binding by Ar = dtbpb, and it saturates at approximately −70 °C. This reduced affinity for O_2 is because the lateral steric bulk of the Ar = dtbpb substituents is so large that it impinges upon the metal center. This weakens the donor strength of the ligand, which increases the $E_{1/2}$ of the $[Cu(dtbpb_3\text{-TMPA})(NCMe)]^{2+/+}$ redox couple relative to the Ar = tpb and dpb complexes, thereby decreasing the driving force for binding O_2. Regardless, the nontraditional employment of steric bulk used in this study provides $Cu^{II}(\eta^1\text{-}O_2^{\bullet-})$ complexes that are fully stable against collapse to the corresponding $Cu^{II}(\mu^2\text{-}O_2^{2-})Cu^{II}$ species. Oxygenation behavior and high $Cu^{II}(\eta^1\text{-}O_2^{\bullet-})$ stability of this type have been previously reported only for Schindler's complex $[Cu^{II}(\eta^1\text{-}O_2^{\bullet-})(TMG_3\text{-tren})]^{+}$.[32,33,93] However, unlike $[Cu^{II}(\eta^1\text{-}O_2^{\bullet-})(TMG_3\text{-tren})]^{+}$, our $[Cu^{II}(\eta^1\text{-}O_2^{\bullet-})(Ar_3\text{-TMPA})]^{+}$ systems display significant reactivity with external substrates.

Although the steric bulk of the aryl substituents in $[Cu^{II}(\eta^1\text{-}O_2^{\bullet-})(Ar_3\text{-TMPA})]^{+}$ is mostly directed away from the metal center, it does have an impact upon reaction with substrates. This is readily apparent from the sluggish reactivity of the Ar = dtbpb complex relative to its Ar = tpb and dpb analogues, and it is likely the origin of the low reactivity of the $[Cu^{II}(\eta^1\text{-}O_2^{\bullet-})(Ar_3\text{-TMPA})]^{+}$ complexes compared with previously published TMPA derivatives. The Eyring parameters measured and Marcus plot of $(k_BT/e)\ln(k_2)$ vs E_{ox} suggest that this may have an enthalpic origin, but at present, it is not clear how this arises from the steric bulk of the Ar substituents. Nonetheless, the high stability of our $[Cu^{II}(\eta^1\text{-}O_2^{\bullet-})(Ar_3\text{-TMPA})]^{+}$ complexes allows us to compensate for this deficiency by performing reactivity studies at higher temperatures.

We have exploited the aforementioned appealing properties by examining the reaction of $[Cu^{II}(\eta^1\text{-}O_2^{\bullet-})(tpb_3\text{-TMPA})]^{+}$ with a wide range of O−H, N−H, and C−H bond substrates. In all cases, reaction was found to proceed via HAT. Evidence for this includes large KIEs for reaction with MeO-ArOH, DPH, and TPH (11.3(8), 19.8(14), and 9.4(7), respectively, at −40 °C); an inability to react with simple electron transfer agents and weak acids; and a "Marcus plot" derived from reaction with a series of 4-substituted 2,6-di-*tert*-butylphenols (X-ArOH) possessing a negative slope of −0.24, which implies a HAT reaction that proceeds with significant charge transfer. The ease of oxidation of MeO-ArOH and DPH allowed measurement of KIEs over a 50 °C temperature window (from −40 to −90 °C). They were found to be effectively constant, with the resulting Arrhenius parameters ($A_H/A_D \gg 1$ and $\Delta E_A \sim 0$) indicating that HAT reaction (for these substrates) proceeds via tunneling of both H and D atoms.

As anticipated, based upon previous precedent and the Marcus cross relation, oxidation of C−H bonds proved to be very challenging relative to O−H and N−H bonds. More specifically, $[Cu^{II}(\eta^1\text{-}O_2^{\bullet-})(tpb_3\text{-TMPA})]^{+}$ is kinetically competent for reaction with diphenylamine (BDE = 89.9 kcal mol^{-1}), which possesses a moderately strong N−H bond but is only able to oxidize substrates containing very weak C−H bonds. Thus, although the rates at which $[Cu^{II}(\eta^1\text{-}O_2^{\bullet-})(tpb_3\text{-TMPA})]^{+}$ reacts with substrates are inversely correlated with the X-H BDEs of the substrates, it is clear that this is not the sole determining factor. Efforts to correlate these observed general trends in reactivity to kinetic barriers (derived from Eyring plots) for reaction with the substrates MeO-ArOH, DPH, TPH, and BNAH did not yield a simple answer. Although the entropy of activation for reaction with BNAH is larger than for the other substrates, the difference is not sufficient to fully explain the observed reactivity differences, and a comparatively large enthalpic barrier is also a contributing factor. Attempts to draw broader and more insightful conclusions are handicapped by the dearth of reports of Eyring parameters for HAT reactions to superoxocopper(II) complexes (or related late transition superoxometal complexes), and it is clear that a more extensive survey of such data would be greatly beneficial.

In summary, we have developed a handful of remarkably stable $Cu^{II}(\eta^1\text{-}O_2^{\bullet-})$ complexes that retain significant reactivity with substrates. This has allowed us to conduct extensive reactivity studies, including rare examples of variable temperature studies. The results obtained provide insight into the inherent reactivity properties of the $Cu^{II}(\eta^1\text{-}O_2^{\bullet-})$ species. Unfortunately, oxidation of moderate-to-high strength C−H bonds remains a serious challenge, and emulation of the hydroxylation chemistry displayed by the noncoupled dinuclear copper enzymes continues to be elusive. The prearrangement and activation of substrates by the secondary structure of the enzymes likely play a major role in facilitating such chemistry. Nevertheless, we believe that there is scope for (and we are working on) enhancing the reactivity of our $[Cu^{II}(\eta^1\text{-}O_2^{\bullet-})(Ar_3\text{-TMPA})]^{+}$ systems via modulation of the ligand steric bulk, which clearly hinders reaction, and moving to higher temperatures, where O_2 binding is less favored but substrate oxidation is more facile.

ASSOCIATED CONTENT

Supporting Information

The Supporting Information is available free of charge at https://pubs.acs.org/doi/10.1021/jacs.1c07837.

Experimental and synthetic procedures, X-ray crystallographic data collection and structural parameters,

https://doi.org/10.1021/jacs.1c07837
J. Am. Chem. Soc. 2021, 143, 19731−19747

additional UV−vis and resonance Raman spectra, and reaction kinetics data (PDF)

Accession Codes

CCDC 1959106, 2094618, and 2094668 contain the supplementary crystallographic data for this paper. These data can be obtained free of charge via www.ccdc.cam.ac.uk/data_request/cif, or by emailing data_request@ccdc.cam.ac.uk, or by contacting The Cambridge Crystallographic Data Centre, 12 Union Road, Cambridge CB2 1EZ, UK; fax: +44 1223 336033.

AUTHOR INFORMATION

Corresponding Author

Jason England − *Division of Chemistry and Biological Chemistry, School of Physical and Mathematical Sciences, Nanyang Technological University, Singapore 637371, Singapore; Department of Chemistry, University of Lincoln, Lincoln LN6 7TW, U.K.;* orcid.org/0000-0002-1525-4105; Email: jengland@lincoln.ac.uk, je197@gmail.com

Authors

Sebastian Y. Quek − *Division of Chemistry and Biological Chemistry, School of Physical and Mathematical Sciences, Nanyang Technological University, Singapore 637371, Singapore*

Suman Debnath − *Division of Chemistry and Biological Chemistry, School of Physical and Mathematical Sciences, Nanyang Technological University, Singapore 637371, Singapore*

Shoba Laxmi − *Division of Chemistry and Biological Chemistry, School of Physical and Mathematical Sciences, Nanyang Technological University, Singapore 637371, Singapore;* orcid.org/0000-0003-2526-7433

Maurice van Gastel − *Max-Planck-Institut für Kohlenforschung, Mülheim an der Ruhr D-45470, Germany;* orcid.org/0000-0002-1547-6365

Tobias Krämer − *Department of Chemistry, Maynooth University, Maynooth, Co. Kildare W23 F2H6, Ireland; Hamilton Institute, Maynooth University, Maynooth, Co. Kildare W23 F2H6, Ireland;* orcid.org/0000-0001-5842-9553

Complete contact information is available at: https://pubs.acs.org/10.1021/jacs.1c07837

Author Contributions

#S.Y.Q., S.D., and S.L. contributed equally.

Notes

The authors declare no competing financial interest.

ACKNOWLEDGMENTS

J.E. is grateful to NTU (M4081442, 000416-00001) and the Ministry of Education of Singapore (AcRF Tier 1 Grant RG8/19 (S), 002689-00001) for funding. We thank Dr. Rakesh Ganguly and Dr. Yongxin Li of the SPMS (NTU) X-ray lab for measurement and refinement of X-ray crystallographic data. In addition, we thank Anchisar Rakthanyakan for help with collecting resonance Raman data. T.K. acknowledges the Irish Centre for High-End Computing (ICHEC) for the provision of computational facilities and support.

REFERENCES

(1) Solomon, E. I.; Heppner, D. E.; Johnston, E. M.; Ginsbach, J. W.; Cirera, J.; Qayyum, M.; Kieber-Emmons, M. T.; Kjaergaard, C. H.; Hadt, R. G.; Tian, L. Copper Active Sites in Biology. *Chem. Rev.* **2014**, *114*, 3659−3853.

(2) Quist, D. A.; Diaz, D. E.; Liu, J. J.; Karlin, K. D. Activation of dioxygen by copper metalloproteins and insights from model complexes. *JBIC, J. Biol. Inorg. Chem.* **2017**, *22*, 253−288.

(3) Whittaker, J. W. Free Radical Catalysis by Galactose Oxidase. *Chem. Rev.* **2003**, *103*, 2347−2364.

(4) Whittaker, M. M.; Whittaker, J. W. Catalytic Reaction Profile for Alcohol Oxidation by Galactose Oxidase. *Biochemistry* **2001**, *40*, 7140−7148.

(5) Whittaker, J. W. Galactose oxidase. In *Advances in Protein Chemistry*; Academic Press, 2002; Vol. *60*, pp 1−49.

(6) Klinman, J. P. Mechanisms Whereby Mononuclear Copper Proteins Functionalize Organic Substrates. *Chem. Rev.* **1996**, *96*, 2541−2561.

(7) Klinman, J. P. The Copper-Enzyme Family of Dopamine β-Monooxygenase and Peptidylglycine α-Hydroxylating Monooxygenase: Resolving the Chemical Pathway for Substrate Hydroxylation. *J. Biol. Chem.* **2006**, *281*, 3013−3016.

(8) Appel, M. J.; Meier, K. K.; Lafrance-Vanasse, J.; Lim, H.; Tsai, C.-L.; Hedman, B.; Hodgson, K. O.; Tainer, J. A.; Solomon, E. I.; Bertozzi, C. R. Formylglycine-generating enzyme binds substrate directly at a mononuclear Cu(I) center to initiate O_2 activation. *Proc. Natl. Acad. Sci. U. S. A.* **2019**, *116*, 5370−5375.

(9) Miarzlou, D. A.; Leisinger, F.; Joss, D.; Häussinger, D.; Seebeck, F. P. Structure of formylglycine-generating enzyme in complex with copper and a substrate reveals an acidic pocket for binding and activation of molecular oxygen. *Chem. Sci.* **2019**, *10*, 7049−7058.

(10) Evans, J. P.; Ahn, K.; Klinman, J. P. Evidence That Dioxygen and Substrate Activation Are Tightly Coupled in Dopamine β-Monooxygenase: Implications for the Reactive Oxygen Species. *J. Biol. Chem.* **2003**, *278*, 49691−49698.

(11) Francisco, W. A.; Merkler, D. J.; Blackburn, N. J.; Klinman, J. P. Kinetic Mechanism and Intrinsic Isotope Effects for the Peptidylglycine α-Amidating Enzyme Reaction. *Biochemistry* **1998**, *37*, 8244−8252.

(12) Tian, G.; Berry, J. A.; Klinman, J. P. Oxygen-18 Kinetic Isotope Effects in the Dopamine β-Monooxygenase Reaction: Evidence for a New Chemical Mechanism in Non-Heme, Metallomonooxygenase. *Biochemistry* **1994**, *33*, 226−234.

(13) Miller, S. M.; Klinman, J. P. Magnitude of Intrinsic Isotope Effects in the Dopamine β-Monooxygenase Reaction. *Biochemistry* **1983**, *22*, 3091−3096.

(14) Hess, C. R.; McGuirl, M. M.; Klinman, J. P. Mechanism of the Insect Enzyme, Tyramine β-Monooxygenase, Reveals Differences from the Mammalian Enzyme, Dopamine β-Monooxygenase. *J. Biol. Chem.* **2008**, *283*, 3042−3049.

(15) Francisco, W. A.; Knapp, M. J.; Blackburn, N. J.; Klinman, J. P. Hydrogen Tunneling in Peptidylglycine α-Hydroxylating Monooxygenase. *J. Am. Chem. Soc.* **2002**, *124*, 8194−8195.

(16) Prigge, S. T.; Eipper, B. A.; Mains, R. E.; Amzel, L. M. Dioxygen Binds End-On to Mononuclear Copper in a Precatalytic Enzyme Complex. *Science* **2004**, *304*, 864−867.

(17) Cowley, R. E.; Tian, L.; Solomon, E. I. Mechanism of O_2 activation and substrate hydroxylation in noncoupled binuclear copper monooxygenases. *Proc. Natl. Acad. Sci. U. S. A.* **2016**, *113*, 12035−12040.

(18) Chen, P.; Solomon, E. I. Oxygen Activation by the Noncoupled Binuclear Copper Site in Peptidylglycine α-Hydroxylating Monooxygenase. Reaction Mechanism and Role of the Noncoupled Nature of the Active Site. *J. Am. Chem. Soc.* **2004**, *126*, 4991−5000.

(19) Elwell, C. E.; Gagnon, N. L.; Neisen, B. D.; Dhar, D.; Spaeth, A. D.; Yee, G. M.; Tolman, W. B. Copper-Oxygen Complexes Revisited: Structures, Spectroscopy, and Reactivity. *Chem. Rev.* **2017**, *117*, 2059−2107.

(20) Mirica, L. M.; Ottenwaelder, X.; Stack, T. D. P. Structure and Spectroscopy of Copper-Dioxygen Complexes. *Chem. Rev.* **2004**, *104*, 1013−1045.
(21) Karlin, K. D.; Wei, N.; Jung, B.; Kaderli, S.; Zuberbuehler, A. D. Kinetic, Thermodynamic, and Spectral Characterization of the Primary Cu-O_2 Adduct in a Reversibly Formed and Structurally Characterized Peroxo-Dicopper(II) Complex. *J. Am. Chem. Soc.* **1991**, *113*, 5868−5870.
(22) Karlin, K. D.; Kaderli, S.; Zuberbühler, A. D. Kinetics and Thermodynamics of Copper(I)/Dioxygen Interaction. *Acc. Chem. Res.* **1997**, *30*, 139−147.
(23) Bhadra, M.; Lee, J. Y. C.; Cowley, R. E.; Kim, S.; Siegler, M. A.; Solomon, E. I.; Karlin, K. D. Intramolecular Hydrogen Bonding Enhances Stability and Reactivity of Mononuclear Cupric Superoxide Complexes. *J. Am. Chem. Soc.* **2018**, *140*, 9042−9045.
(24) Fujisawa, K.; Tanaka, M.; Moro-Oka, Y.; Kitajima, N. A Monomeric Side-On Superoxocopper(II) Complex: Cu(O_2)(HB(3-tBu-5-iPrpz)$_3$). *J. Am. Chem. Soc.* **1994**, *116*, 12079−12080.
(25) Aboelella, N. W.; Lewis, E. A.; Reynolds, A. M.; Brennessel, W. W.; Cramer, C. J.; Tolman, W. B. Snapshots of Dioxygen Activation by Copper: The Structure of a 1:1 Cu/O_2 Adduct and Its Use in Syntheses of Asymmetric Bis(s-oxo) Complexes. *J. Am. Chem. Soc.* **2002**, *124*, 10660−10661.
(26) Reynolds, A. M.; Gherman, B. F.; Cramer, C. J.; Tolman, W. B. Characterization of a 1:1 Cu-O_2 Adduct Supported by an Anilido Imine Ligand. *Inorg. Chem.* **2005**, *44*, 6989−6997.
(27) Iovan, D. A.; Wrobel, A. T.; McClelland, A. A.; Scharf, A. B.; Edouard, G. A.; Betley, T. A. Reactivity of a stable copper-dioxygen complex. *Chem. Commun.* **2017**, *53*, 10306−10309.
(28) Aboelella, N. W.; Kryatov, S. V.; Gherman, B. F.; Brennessel, W. W.; Young, V. G., Jr.; Sarangi, R.; Rybak-Akimova, E. V.; Hodgson, K. O.; Hedman, B.; Solomon, E. I.; Cramer, C. J.; Tolman, W. B. Dioxygen Activation at a Single Copper Site: Structure, Bonding, and Mechanism of Formation of 1:1 Cu-O_2 Adducts. *J. Am. Chem. Soc.* **2004**, *126*, 16896−16911.
(29) Spencer, D. J. E.; Aboelella, N. W.; Reynolds, A. M.; Holland, P. L.; Tolman, W. B. β-Diketiminate Ligand Backbone Structural Effects on Cu(I)/O_2 Reactivity: Unique Copper-Superoxo and Bis(μ-oxo) Complexes. *J. Am. Chem. Soc.* **2002**, *124*, 2108−2109.
(30) Chen, P.; Root, D. E.; Campochiaro, C.; Fujisawa, K.; Solomon, E. I. Spectroscopic and Electronic Structure Studies of the Diamagnetic Side-On CuII-Superoxo Complex Cu(O_2)[HB(3-R-5-^{i}Prpz)$_3$]: Antiferromagnetic Coupling versus Covalent Delocalization. *J. Am. Chem. Soc.* **2003**, *125*, 466−474.
(31) Schatz, M.; Raab, V.; Foxon, S. P.; Brehm, G.; Schneider, S.; Reiher, M.; Holthausen, M. C.; Sundermeyer, J.; Schindler, S. Combined Spectroscopic and Theoretical Evidence for a Persistent End-On Copper Superoxo Complex. *Angew. Chem., Int. Ed.* **2004**, *43*, 4360−4363.
(32) Würtele, C.; Gaoutchenova, E.; Harms, K.; Holthausen, M. C.; Sundermeyer, J.; Schindler, S. Crystallographic Characterization of a Synthetic 1:1 End-On Copper Dioxygen Adduct Complex. *Angew. Chem., Int. Ed.* **2006**, *45*, 3867−3869.
(33) Lanci, M. P.; Smirnov, V. V.; Cramer, C. J.; Gauchenova, E. V.; Sundermeyer, J.; Roth, J. P. Isotopic Probing of Molecular Oxygen Activation at Copper(I) Sites. *J. Am. Chem. Soc.* **2007**, *129*, 14697−14709.
(34) Kobayashi, Y.; Ohkubo, K.; Nomura, T.; Kubo, M.; Fujieda, N.; Sugimoto, H.; Fukuzumi, S.; Goto, K.; Ogura, T.; Itoh, S. Copper(I)-Dioxygen Reactivity in a Sterically Demanding Tripodal Tetradentate tren Ligand: Formation and Reactivity of a Mononuclear Copper(II) End-On Superoxo Complex. *Eur. J. Inorg. Chem.* **2012**, *2012*, 4574−4578.
(35) Donoghue, P. J.; Gupta, A. K.; Boyce, D. W.; Cramer, C. J.; Tolman, W. B. An Anionic, Tetragonal Copper(II) Superoxide Complex. *J. Am. Chem. Soc.* **2010**, *132*, 15869−15871.
(36) Maiti, D.; Lee, D.-H.; Gaoutchenova, K.; Würtele, C.; Holthausen, M. C.; Narducci Sarjeant, A. A.; Sundermeyer, J.; Schindler, S.; Karlin, K. D. Reactions of a Copper(II) Superoxo Complex Lead to C-H and O-H Substrate Oxygenation: Modeling Copper-Monooxygenase C-H Hydroxylation. *Angew. Chem., Int. Ed.* **2008**, *47*, 82−85.
(37) Bailey, W. D.; Dhar, D.; Cramblitt, A. C.; Tolman, W. B. Mechanistic Dichotomy in Proton-Coupled Electron-Transfer Reactions of Phenols with a Copper Superoxide Complex. *J. Am. Chem. Soc.* **2019**, *141*, 5470−5480.
(38) Bailey, W. D.; Gagnon, N. L.; Elwell, C. E.; Cramblitt, A. C.; Bouchey, C. J.; Tolman, W. B. Revisiting the Synthesis and Nucleophilic Reactivity of an Anionic Copper Superoxide Complex. *Inorg. Chem.* **2019**, *58*, 4706−4711.
(39) Pirovano, P.; Magherusan, A. M.; McGlynn, C.; Ure, A.; Lynes, A.; McDonald, A. R. Nucleophilic Reactivity of a Copper(II)-Superoxide Complex. *Angew. Chem., Int. Ed.* **2014**, *53*, 5946−5950.
(40) Itoh, S. Developing Mononuclear Copper-Active-Oxygen Complexes Relevant to Reactive Intermediates of Biological Oxidation Reactions. *Acc. Chem. Res.* **2015**, *48*, 2066−2074.
(41) Tano, T.; Okubo, Y.; Kunishita, A.; Kubo, M.; Sugimoto, H.; Fujieda, N.; Ogura, T.; Itoh, S. Redox Properties of a Mononuclear Copper(II)-Superoxide Complex. *Inorg. Chem.* **2013**, *52*, 10431−10437.
(42) Kunishita, A.; Kubo, M.; Sugimoto, H.; Ogura, T.; Sato, K.; Takui, T.; Itoh, S. Mononuclear Copper(II)-Superoxo Complexes that Mimic the Structure and Reactivity of the Active Centers of PHM and DβM. *J. Am. Chem. Soc.* **2009**, *131*, 2788−2789.
(43) Kunishita, A.; Ertem, M. Z.; Okubo, Y.; Tano, T.; Sugimoto, H.; Ohkubo, K.; Fujieda, N.; Fukuzumi, S.; Cramer, C. J.; Itoh, S. Active Site Models for the Cu_A Site of Peptidylglycine α-Hydroxylating Monooxygenase and Dopamine β-Monooxygenase. *Inorg. Chem.* **2012**, *51*, 9465−9480.
(44) Zhang, C. X.; Kaderli, S.; Costas, M.; Kim, E.-i.; Neuhold, Y.-M.; Karlin, K. D.; Zuberbühler, A. D. Copper(I)-Dioxygen Reactivity of [(L)Cu^I]$^+$ (L = Tris(2-pyridylmethyl)amine): Kinetic/ Thermodynamic and Spectroscopic Studies Concerning the Formation of Cu-O_2 and Cu_2-O_2 Adducts as a Function of Solvent Medium and 4-Pyridyl Ligand Substituent Variations. *Inorg. Chem.* **2003**, *42*, 1807−1824.
(45) Maiti, D.; Fry, H. C.; Woertink, J. S.; Vance, M. A.; Solomon, E. I.; Karlin, K. D. A 1:1 Copper-Dioxygen Adduct is an End-on Bound Superoxo Copper(II) Complex which Undergoes Oxygenation Reactions with Phenols. *J. Am. Chem. Soc.* **2007**, *129*, 264−265.
(46) Lee, J. Y.; Peterson, R. L.; Ohkubo, K.; Garcia-Bosch, I.; Himes, R. A.; Woertink, J.; Moore, C. D.; Solomon, E. I.; Fukuzumi, S.; Karlin, K. D. Mechanistic Insights into the Oxidation of Substituted Phenols via Hydrogen Atom Abstraction by a Cupric-Superoxo Complex. *J. Am. Chem. Soc.* **2014**, *136*, 9925−9937.
(47) Peterson, R. L.; Himes, R. A.; Kotani, H.; Suenobu, T.; Tian, L.; Siegler, M. A.; Solomon, E. I.; Fukuzumi, S.; Karlin, K. D. Cupric Superoxo-Mediated Intermolecular C-H Activation Chemistry. *J. Am. Chem. Soc.* **2011**, *133*, 1702−1705.
(48) Diaz, D. E.; Quist, D. A.; Herzog, A. E.; Schaefer, A. W.; Kipouros, I.; Bhadra, M.; Solomon, E. I.; Karlin, K. D. Impact of Intramolecular Hydrogen Bonding on the Reactivity of Cupric Superoxide Complexes with O-H and C-H Substrates. *Angew. Chem., Int. Ed.* **2019**, *58*, 17572−17576.
(49) Addison, A. W.; Rao, T. N.; Reedijk, J.; van Rijn, J.; Verschoor, G. C. Synthesis, structure, and spectroscopic properties of copper(II) compounds containing nitrogen-sulphur donor ligands; the crystal and molecular structure of aqua[1,7-bis(*N*-methylbenzimidazol-2●-yl)-2,6-dithiaheptane]copper(II) perchlorate. *J. Chem. Soc., Dalton Trans.* **1984**, 1349−1356.
(50) Kunishita, A.; Kubo, M.; Ishimaru, H.; Ogura, T.; Sugimoto, H.; Itoh, S. H_2O_2-Reactivity of Copper(II) Complexes Supported by Tris[(pyridin-2-yl)methyl]amine Ligands with 6-Phenyl Substituents. *Inorg. Chem.* **2008**, *47*, 12032−12039.
(51) Chuang, C.-l.; Lim, K.; Chen, Q.; Zubieta, J.; Canary, J. W. Synthesis, Cyclic Voltammetry, and x-ray Crystal Structures of Copper(I) and Copper(II) Complexes of Tris((6-phenyl-2-pyridyl)-methyl)amine (TPPA). *Inorg. Chem.* **1995**, *34*, 2562−2568.

https://doi.org/10.1021/jacs.1c07837
J. Am. Chem. Soc. 2021, 143, 19731−19747

(52) Woertink, J. S.; Tian, L.; Maiti, D.; Lucas, H. R.; Himes, R. A.; Karlin, K. D.; Neese, F.; Würtele, C.; Holthausen, M. C.; Bill, E.; Sundermeyer, J.; Schindler, S.; Solomon, E. I. Spectroscopic and Computational Studies of an End-on Bound Superoxo-Cu(II) Complex: Geometric and Electronic Factors That Determine the Ground State. *Inorg. Chem.* **2010**, *49*, 9450−9459.
(53) Ginsbach, J. W.; Peterson, R. L.; Cowley, R. E.; Karlin, K. D.; Solomon, E. I. Correlation of the Electronic and Geometric Structures in Mononuclear Copper(II) Superoxide Complexes. *Inorg. Chem.* **2013**, *52*, 12872−12874.
(54) Peterson, R. L.; Ginsbach, J. W.; Cowley, R. E.; Qayyum, M. F.; Himes, R. A.; Siegler, M. A.; Moore, C. D.; Hedman, B.; Hodgson, K. O.; Fukuzumi, S.; Solomon, E. I.; Karlin, K. D. Stepwise Protonation and Electron-Transfer Reduction of a Primary Copper-Dioxygen Adduct. *J. Am. Chem. Soc.* **2013**, *135*, 16454−16467.
(55) Falivene, L.; Credendino, R.; Poater, A.; Petta, A.; Serra, L.; Oliva, R.; Scarano, V.; Cavallo, L. SambVca 2. A Web Tool for Analyzing Catalytic Pockets with Topographic Steric Maps. *Organometallics* **2016**, *35*, 2286−2293.
(56) Poater, A.; Ragone, F.; Mariz, R.; Dorta, R.; Cavallo, L. Comparing the Enantioselective Power of Steric and Electrostatic Effects in Transition-Metal-Catalyzed Asymmetric Synthesis. *Chem. - Eur. J.* **2010**, *16*, 14348−14353.
(57) Tyeklar, Z.; Jacobson, R. R.; Wei, N.; Murthy, N. N.; Zubieta, J.; Karlin, K. D. Reversible reaction of dioxygen (and carbon monoxide) with a copper(I) complex. X-ray structures of relevant mononuclear Cu(I) precursor adducts and the *trans*-(μ-1,2-peroxo)-dicopper(II) product. *J. Am. Chem. Soc.* **1993**, *115*, 2677−2689.
(58) Jacobson, R. R.; Tyeklar, Z.; Farooq, A.; Karlin, K. D.; Liu, S.; Zubieta, J. A Cu_2-O_2 complex. Crystal Structure and Characterization of a Reversible Dioxygen Binding System. *J. Am. Chem. Soc.* **1988**, *110*, 3690−3692.
(59) Dahl, E. W.; Dong, H. T.; Szymczak, N. K. Phenylamino derivatives of tris(2-pyridylmethyl)amine: hydrogen-bonded peroxodicopper complexes. *Chem. Commun.* **2018**, *54*, 892−895.
(60) Bordwell, F. G.; Zhang, X.-M. Acidities and homolytic bond dissociation enthalpies of 4-substituted-2,6-di-tert-butylphenols. *J. Phys. Org. Chem.* **1995**, *8*, 529−535.
(61) Wu, T.; MacMillan, S. N.; Rajabimoghadam, K.; Siegler, M. A.; Lancaster, K. M.; Garcia-Bosch, I. Structure, Spectroscopy, and Reactivity of a Mononuclear Copper Hydroxide Complex in Three Molecular Oxidation States. *J. Am. Chem. Soc.* **2020**, *142*, 12265−12276.
(62) Kim, S.; Saracini, C.; Siegler, M. A.; Drichko, N.; Karlin, K. D. Coordination Chemistry and Reactivity of a Cupric Hydroperoxide Species Featuring a Proximal H-Bonding Substituent. *Inorg. Chem.* **2012**, *51*, 12603−12605.
(63) Choi, Y. J.; Cho, K.-B.; Kubo, M.; Ogura, T.; Karlin, K. D.; Cho, J.; Nam, W. Spectroscopic and computational characterization of Cu^{II}-OOR (R = H or cumyl) complexes bearing a Me_6-tren ligand. *Dalton Trans.* **2011**, *40*, 2234−2241.
(64) Yamaguchi, S.; Nagatomo, S.; Kitagawa, T.; Funahashi, Y.; Ozawa, T.; Jitsukawa, K.; Masuda, H. Copper Hydroperoxo Species Activated by Hydrogen-Bonding Interaction with Its Distal Oxygen. *Inorg. Chem.* **2003**, *42*, 6968−6970.
(65) Wada, A.; Harata, M.; Hasegawa, K.; Jitsukawa, K.; Masuda, H.; Mukai, M.; Kitagawa, T.; Einaga, H. Structural and Spectroscopic Characterization of a Mononuclear Hydroperoxo-Copper(II) Complex with Tripodal Pyridylamine Ligands. *Angew. Chem., Int. Ed.* **1998**, *37*, 798−799.
(66) Kunishita, A.; Scanlon, J. D.; Ishimaru, H.; Honda, K.; Ogura, T.; Suzuki, M.; Cramer, C. J.; Itoh, S. Reactions of Copper(II)-H_2O_2 Adducts Supported by Tridentate Bis(2-pyridylmethyl)amine Ligands: Sensitivity to Solvent and Variations in Ligand Substitution. *Inorg. Chem.* **2008**, *47*, 8222−8232.
(67) Warren, J. J.; Tronic, T. A.; Mayer, J. M. Thermochemistry of Proton-Coupled Electron Transfer Reagents and its Implications. *Chem. Rev.* **2010**, *110*, 6961−7001.
(68) Zhu, X.-Q.; Zhang, M.-T.; Yu, A.; Wang, C.-H.; Cheng, J.-P. Hydride, Hydrogen Atom, Proton, and Electron Transfer Driving Forces of Various Five-Membered Heterocyclic Organic Hydrides and Their Reaction Intermediates in Acetonitrile. *J. Am. Chem. Soc.* **2008**, *130*, 2501−2516.
(69) Osako, T.; Ohkubo, K.; Taki, M.; Tachi, Y.; Fukuzumi, S.; Itoh, S. Oxidation Mechanism of Phenols by Dicopper-Dioxygen (Cu_2/O_2) Complexes. *J. Am. Chem. Soc.* **2003**, *125*, 11027−11033.
(70) Fukuzumi, S.; Shimoosako, K.; Suenobu, T.; Watanabe, Y. Mechanisms of Hydrogen-, Oxygen-, and Electron-Transfer Reactions of Cumylperoxyl Radical. *J. Am. Chem. Soc.* **2003**, *125*, 9074−9082.
(71) Ram, M. S.; Hupp, J. T. Linear Free Energy Relations for Multielectron Transfer Kinetics: A Brief Look at the Brønsted/Tafel Analogy. *J. Phys. Chem.* **1990**, *94*, 2378−2380.
(72) Weatherly, S. C.; Yang, I. V.; Thorp, H. H. Proton-Coupled Electron Transfer in Duplex DNA: Driving Force Dependence and Isotope Effects on Electrocatalytic Oxidation of Guanine. *J. Am. Chem. Soc.* **2001**, *123*, 1236−1237.
(73) Guttenplan, J. B.; Cohen, S. G. Triplet Energies, Reduction Potentials, and Ionization Potentials in Carbonyl-Donor Partial Charge-Transfer Interactions. I. *J. Am. Chem. Soc.* **1972**, *94*, 4040−4042.
(74) Wagner, P. J.; Lam, H. M. H. Charge-Transfer Quenching of Triplet r>-Trifluoroacetophenones. *J. Am. Chem. Soc.* **1980**, *102*, 4167−4172.
(75) Connelly, N. G.; Geiger, W. E. Chemical Redox Agents for Organometallic Chemistry. *Chem. Rev.* **1996**, *96*, 877−910.
(76) Kochi, J. K. *Free Radicals*; Wiley: New York, 1973.
(77) Halliwell, B.; Gutteridge, J. M. C. *Free Radicals in Biology and Medicine*, 5th ed.; Oxford University Press: Oxford, U.K., 2015; p 944.
(78) Mayer, J. M. Understanding Hydrogen Atom Transfer: From Bond Strengths to Marcus Theory. *Acc. Chem. Res.* **2011**, *44*, 36−46.
(79) Roth, J. P.; Yoder, J. C.; Won, T. J.; Mayer, J. M. Application of the Marcus Cross Relation to Hydrogen Atom Transfer Reactions. *Science* **2001**, *294*, 2524−2526.
(80) Warren, J. J.; Mayer, J. M. Predicting organic hydrogen atom transfer rate constants using the Marcus cross relation. *Proc. Natl. Acad. Sci. U. S. A.* **2010**, *107*, 5282−5287.
(81) Sutin, N. Theory of Electron Transfer Reactions: Insights and Hindsights. *Prog. Inorg. Chem.* **2007**, *30*, 441−498.
(82) Mayer, J. M Proton-Coupled Electron Transfer: A Reaction Chemist's View. *Annu. Rev. Phys. Chem.* **2004**, *55*, 363−390.
(83) Kindermann, N.; Günes, C.-J.; Dechert, S.; Meyer, F. Hydrogen Atom Abstraction Thermodynamics of a μ-1,2-Superoxo Dicopper-(II) Complex. *J. Am. Chem. Soc.* **2017**, *139*, 9831−9834.
(84) Dhar, D.; Yee, G. M.; Spaeth, A. D.; Boyce, D. W.; Zhang, H.; Dereli, B.; Cramer, C. J.; Tolman, W. B. Perturbing the Copper(III)-Hydroxide Unit through Ligand Structural Variation. *J. Am. Chem. Soc.* **2016**, *138*, 356−368.
(85) Donoghue, P. J.; Tehranchi, J.; Cramer, C. J.; Sarangi, R.; Solomon, E. I.; Tolman, W. B. Rapid C-H Bond Activation by a Monocopper(III)-Hydroxide Complex. *J. Am. Chem. Soc.* **2011**, *133*, 17602−17605.
(86) Sacramento, J. J. D.; Goldberg, D. P. The hydrogen atom transfer reactivity of a porphyrinoid cobalt superoxide complex. *Chem. Commun.* **2019**, *55*, 913−916.
(87) Devi, T.; Lee, Y.-M.; Jung, J.; Sankaralingam, M.; Nam, W.; Fukuzumi, S. A Chromium(III)-Superoxo Complex as a Three-Electron Oxidant with a Large Tunneling Effect in Multi-Electron Oxidation of NADH Analogues. *Angew. Chem., Int. Ed.* **2017**, *56*, 3510−3515.
(88) Knapp, M. J.; Rickert, K.; Klinman, J. P. Temperature-Dependent Isotope Effects in Soybean Lipoxygenase-1: Correlating Hydrogen Tunneling with Protein Dynamics. *J. Am. Chem. Soc.* **2002**, *124*, 3865−3874.
(89) Klinman, J. P.; Offenbacher, A. R. Understanding Biological Hydrogen Transfer Through the Lens of Temperature Dependent Kinetic Isotope Effects. *Acc. Chem. Res.* **2018**, *51*, 1966−1974.

https://doi.org/10.1021/jacs.1c07837
J. Am. Chem. Soc. 2021, 143, 19731−19747

(90) Kohen, A.; Klinman, J. P. Enzyme Catalysis: Beyond Classical Paradigms. *Acc. Chem. Res.* **1998**, *31*, 397−404.
(91) Kwart, H. Temperature Dependence of the Primary Kinetic Hydrogen Isotope Effect as a Mechanistic Criterion. *Acc. Chem. Res.* **1982**, *15*, 401−408.
(92) Cho, J.; Woo, J.; Nam, W. An "End-On" Chromium(III)-Superoxo Complex: Crystallographic and Spectroscopic Characterization and Reactivity in C-H Bond Activation of Hydrocarbons. *J. Am. Chem. Soc.* **2010**, *132*, 5958−5959.
(93) Bhadra, M.; Transue, W. J.; Lim, H.; Cowley, R. E.; Lee, J. Y. C.; Siegler, M. A.; Josephs, P.; Henkel, G.; Lerch, M.; Schindler, S.; Neuba, A.; Hodgson, K. O.; Hedman, B.; Solomon, E. I.; Karlin, K. D. A Thioether-Ligated Cupric Superoxide Model with Hydrogen Atom Abstraction Reactivity. *J. Am. Chem. Soc.* **2021**, *143*, 3707−3713.

https://doi.org/10.1021/jacs.1c07837
J. Am. Chem. Soc. 2021, 143, 19731−19747